

Single Wall Carbon Nanotube/Polyacrylonitrile Composite Fiber

A Thesis

Presented to

The Academic Faculty

By

Jianghong Liang

In Partial Fulfillment

Of the Requirements for the Degree

Master of Science in Polymer, Textile and Fiber Engineering

Georgia Institute of Technology

October, 2004

Single Wall Carbon Nanotube/Polyacrylonitrile Composite Fiber

Approved By

Dr. Satish Kumar, Chairman

Dr. Fred L. Cook

Dr. Mary Lynn Realff

Date Approved: October 7, 2004

ACKNOWLEDGEMENT

This thesis was completed under the encouragement and guidance of my advisor, Dr. Satish Kumar, who has given me great amount of support during this research. I would like to thank Dr. T.V. Sreekumar who has generously given me his experience in fiber spinning and polymer chemistry. I would like to thank Dr. Tao Liu for his patient help and suggestions and my group fellows, Xiefei Zhang, Hongming Ma, Huina Guo, Tong Wang, Chongfu Zhou, Jing Liu, Dr.Young-Bin Park, for their help through the whole duration of my work.

I would like to thank Dr. Jim Tour of Rice University and his research group for providing the benzonitrile functionalized SWNT samples, my thesis committee members, Dr. Fred L. Cook and Dr. Mary Lynn Realff, who have given their precious suggestions and help.

Finally, I thank my father Faxun Liang who constantly offers me his own scientific research experience and methodology and always encourages me to overcome any hardships in life; my mother Jiajing Zheng for her love and care; as well as my whole family who has sacrificed so much for my studies.

TABLE OF CONTENTS

ACKNOWLEDGEMENT	iii
LIST OF TABLES	vii
LIST OF FIGURES.....	viii
LIST OF SYMBOLS AND ABBREVIATIONS	x
SUMMARY	xii
CHAPTER 1 INTRODUCTION.....	1
1.1 Carbon Materials.....	1
1.1.1 Diamond and Graphite	1
1.1.2 Carbon Graphite Whiskers	3
1.1.3 Carbon Black	3
1.1.4 Fullerenes and Carbon Nanotubes	4
1.1.5 Structure and Properties of Single Wall Carbon Nanotubes	4
1.1.6 Potential Applications of SWNTs.....	9
1.2 Polyacrylonitrile	10
1.3 Composite Fiber.....	10
1.4 SWNT Functionalization.....	11
1.5 Objectives.....	12
CHAPTER 2 EXPERIMENTAL	13
2.1 General Procedure.....	13
2.2 Non-acid Treated SWNT/PAN Dope	14
2.3 Nitric Acid Treatment of SWNTs.....	15
2.4 Nitric Acid Treated SWNT/PAN Dope	16

2.5	SWNT/PAN Fiber Spinning.....	16
2.6	Benzonitrile Functionalized SWNTs/PAN Composite Fiber.....	18
2.6.1	Benzonitrile Functionalized SWNTs	18
2.6.2	PAN from Exlan Inc. (Japan)	19
2.6.3	Benzonitrile Functionalized SWNT/PAN Fiber Spinning	21
CHAPTER 3	CHARACTERIZATION AND ANALYSIS.....	22
3.1	SWNT/PAN Composite Fiber	22
3.1.1	Geometric Properties.....	22
3.1.2	Tensile Test and Dynamic Mechanical Analysis.....	23
3.1.3	Thermo-Mechanical Analysis (Shrinkage).....	25
3.1.4	Differential Scanning Calorimetry (DSC).....	27
3.1.5	FTIR Spectra.....	28
3.1.6	Raman Spectra	30
3.1.7	Wide Angle X-ray Diffraction Pattern (WAXD).....	32
3.2	SWNT/PAN Composite Fiber Orientation	35
3.2.1	SWNTs Orientation.....	35
3.2.2	PAN Molecule Orientation	37
3.3	SWNT/PAN Fiber Modulus.....	37
3.4	Benzonitrile Functionalized SWNT/PAN Composite Fiber	40
3.4.1	Geometric Properties.....	40
3.4.2	Tensile Test and Dynamic Mechanical Analysis.....	42
3.4.3	Thermo-Mechanical Analysis (Shrinkage).....	43
3.4.4	Thermo-gravimetric Analysis	44

3.4.5	Raman Spectra	45
3.4.6	WAXD.....	46
CHAPTER 4	CONCLUSIONS AND RECOMMENDATIONS	49
4.1	Conclusions	49
4.2	Recommendations for Future Work.....	50
APPENDIX A: MATLAB PROGRAM FOR CALCULATING SWNTS		
	ORIENTATION FUNCTION FROM RAMAN SPECTRA	52
	REFERENCES.....	54

LIST OF TABLES

Table 1.1 Mechanical Properties of SWNT Ropes	7
Table 1.2 Physical Properties of SWNTs	8
Table 2.1 Spinning conditions for SWNT/PAN composite fiber	17
Table 2.2 FTIR Absorption Peaks and Assignments for Exlan PAN	21
Table 3.1 Tensile properties of PAN and SWNT/PAN composite fibers	23
Table 3.2 The G band peak value $I_{vv}(\varphi)$ of SWNT/Fibers	32
Table 3.3 PAN lattice data of control PAN and SWNT/PAN fibers	34
Table 3.4 The mechanical properties of SWNT ropes ⁵⁸	38
Table 3.5 Comparison of experimental data and predicted values	39
Table 3.6 Tensile properties of functionalized composite fibers	42
Table 3.7 Lattice parameters of Functionalized SWNT/PAN Fibers.....	48

LIST OF FIGURES

Figure 1.1 Various Forms of Carbon.....	1
Figure 1.2 (a) Crystal Graphite and (b) Diamond crystal.....	2
Figure 1.3 (a) Carbon Whiskers and (b) Carbon Black.	3
Figure 1.4 Schematic of a graphene sheet illustrating lattice vectors.	5
Figure 1.5 Atomic structure of SWNTs: (a) zigzag and (b) armchair. ¹¹	5
Figure 1.6 Rope Assembly of SWNTs. ¹⁴	7
Figure 2.1 SWNT/PAN dope preparation setup.	14
Figure 2.2 Optical Micrographs of (a) non-acid treated , (b) nitric acid treated SWNT/PAN dope.....	16
Figure 2.3 Fiber spinning setup.....	18
Figure 2.4 Functionalized SWNTs: (a) JLH-II-085 SWNTs and (b) Js-2-88 SWNTs.	19
Figure 2.5 Viscosity data of Exlan PAN.	19
Figure 2.6 FTIR pattern of Exlan PAN sample powder.	20
Figure 2.7 Optical micrographs of (a) JLH-II-085/PAN and (b) JS-2-88/PAN Dope.....	21
Figure 3.1 SEM images of (a) Non-acid treated SWNT/PAN, (b) Acid treated SWNT/PAN.	22
Figure 3.2 Storage moduli of control PAN and SWNT/PAN fibers.....	24
Figure 3.3 Loss moduli of control PAN and SWNT/PAN fibers.	24
Figure 3.4 Loss tangent of control PAN and SWNT/PAN fibers.	25
Figure 3.5 TMA of control PAN and SWNT/PAN fibers.	26
Figure 3.6 Thermal shrinkage in a) PAN, b) SWNT/PAN (5:95) and c) SWNT/PAN (10:90) composite fiber as a function of temperature. ⁴⁷	27

Figure 3.7 DSC of control PAN and SWNT/PAN fibers.....	28
Figure 3.8 FTIR spectra of PAN and PAN fibers.....	29
Figure 3.9 SWNT's atomic vibrations for (a) the RBM and (b) the G band modes.....	30
Figure 3.10 Raman spectra of SWNT/PAN fibers.....	31
Figure 3.11 WAXD patterns of (a) control PAN, (b) non-acid treated SWNT/PAN and (c) acid treated SWNT/PAN fibers.....	33
Figure 3.12 Equatorial WAXD scan of SWNT/PAN fibers.....	33
Figure 3.13 Azimuthal WAXD scan of SWNT/PAN fibers.....	34
Figure 3.14 The Spools of (a) Exlan PAN, (b) JLH-II-085/PAN and (c) JS-2-88/PAN fiber.....	40
Figure 3.15 SEM image of functionalized fibers. (a) Exlan PAN, (b) JLH-II-085/PAN, (c) JS-2-88/PAN.....	41
Figure 3.16 Storage modulus of benzonitrile functionalized SWNT/PAN fibers.....	42
Figure 3.17 Loss tangent of functionalized SWNT/PAN fibers.....	43
Figure 3.18 TMA of benzonitrile functionalized SWNT/PAN fibers.....	44
Figure 3.19 TGA test of functionalized SWNT/PAN fibers.....	45
Figure 3.20 Raman spectra of functionalized SWNT/PN fibers.....	46
Figure 3.21 WAXD patterns of functionalized fibers. (a) Exlan PAN, (b) JLH-II- 085/PAN, (c) JS-2-88/PAN.....	46
Figure 3.22 Equatorial WAXD scan of functionalized SWNT/PAN fibers.....	47
Figure 3.23 Azimuthal WAXD scan of functionalized SWNT/PAN fibers.....	48

LIST OF SYMBOLS AND ABBREVIATIONS

SWNT	Single Wall Carbon Nanotube
PAN	polyacrylonitrile
SEM	scanning electron micrograph
TEM	transmission electron micrograph
FTIR	fourier transform infra red spectra
WAXD	wide angle x-ray diffraction
TMA	thermo-mechanical analysis
TGA	thermo-gravimeter analysis
DSC	differential scanning calorimeter
DMA	dynamic mechanical analysis
GPa	giga pascal (10^9 pascal)
MPa	mega pascal (10^6 pascal)
TPa	tera pascal (10^{12} pascal)
C_h	chiral vector of carbon nanotube
$[\eta]$	intrinsic viscosity
(M_v)	viscosity averaged molecular weight
E_{11}	electron energy at level 11
E_{laser}	energy of incident laser light
φ	the angle between the fiber and the polarizer
$I_{vv}(\varphi)$	the G band peak intensity when fiber is at φ with the polarizer
K	proportional constant
$I_R(e_{s//}, \theta, \varphi)$	scattering light intensity of an individual SWNT

$e_{s//}$	scattering coefficient
α_{zz}	the polarizability at zz direction of an individual SWNT
θ	the angle between an individual SWNT and the fiber axis
$F(\theta)$	the orientation distribution function with respect to θ
w	Full width at half maximum of the distribution function $F(\theta)$
$\langle \cos^2 \theta \rangle$	the average value of $\cos^2 \theta$ over all θ values
f	Herman's orientation factor
$\varphi_{z,hkl}$	the angle between crystal plane hkl and z axis
$\langle \cos^2 \varphi_{z,hkl} \rangle$	the average value of $\cos^2 \varphi_{z,hkl}$
E_1	the Young's modulus along the SWNT rope axis
E_2	the Young's modulus along the SWNT rope's radial directions
G_{12}	the shearing modulus in the plane perpendicular to the rope axis
σ	the breakage strength along the SWNT rope axis
ν_{12}	Poisson ratio
V_{SWNT}	volume fractions of SWNTs in the composite fiber
V_{PAN}	volume fraction of PAN in the composite fiber
E_{SWNT}	modulus of SWNTs
E_{PAN}	modulus of PAN
E_{Fiber}	modulus of composite fiber

SUMMARY

Single Wall Carbon Nanotubes (SWNTs), discovered in 1993, have good mechanical, electrical and thermal properties. Polyacrylonitrile (PAN) is an important fiber for textiles as well as a precursor for carbon fibers. PAN has been produced since 1930s.

In this study, we have processed SWNT/PAN fibers by dry-jet wet spinning. Purified SWNT, nitric acid treated SWNTs, and benzonitrile functionalized SWNTs have been used. Fiber processing was done in Dimethyl Formamide (DMF) and coagulation was done in DMF/water mixture. The coagulated fibers were drawn (draw ratio of 6) at 95 °C.

Structure, orientation, and mechanical properties of these fibers have been studied. The cross-sections for all the fibers are not circular. Incorporation of SWNT in PAN results in improved mechanical properties, tensile modulus increased from 7.9 GPa for control PAN to 13.7 GPa for SWNT/PAN composite fiber, and functionalized SWNTs result in higher improvements with tensile modulus reaching 17.8 GPa for acid treated SWNT/PAN composite fibers. The theoretical analysis suggests that observed moduli of the composite fibers are consistent with the predicted values.

CHAPTER 1 INTRODUCTION

1.1 Carbon Materials

Carbon is the lightest atom in column IV of the periodic table and is an element with unique properties. It can exist in various forms as given in Figure 1.1.

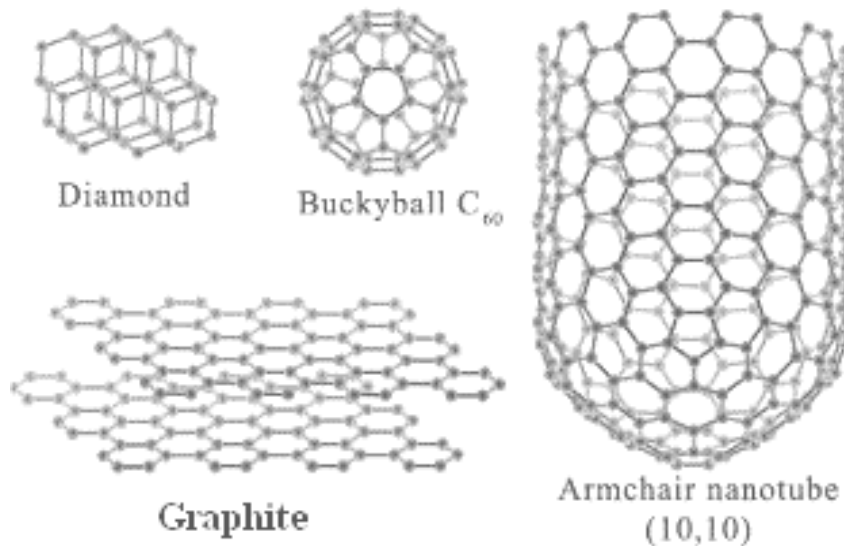
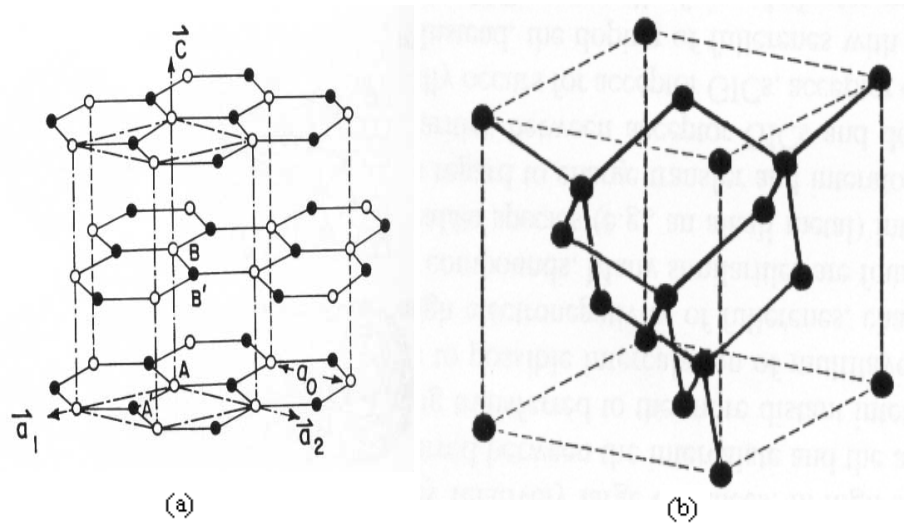


Figure 1.1 Various Forms of Carbon.¹

1.1.1 Diamond and Graphite

Diamond is a three-dimensional isotropic material with sp^3 bonding. Graphite has a two-dimensional hexagonal structure with sp^2 bonding and is highly anisotropic. The crystal structures of diamond and graphite are given in Figure 1.2. Commonly used graphite materials are natural crystal flakes that are found around the world. The natural

crystal flakes can be as large as several millimeters along the basal plane, but are typically much less than 0.1 mm in thickness perpendicular to the basal planes. The very small size restricts the use of natural flakes for various scientific studies and applications.²



Synthetic crystal graphite called kish graphite is commonly used in scientific investigations because of the larger size of the flakes and higher structural perfection. Kish graphite crystals form on the surface of high carbon content iron melts and are harvested as crystals from such solutions. Recently some new precursors such as polyimide and polyoxadiazole resins have been used to synthesize graphite films, and after suitable pyrolyzing and heat treatment steps, these carbon films show an improved 3D ordering and quality.

1.1.2 Carbon Graphite Whiskers

Graphite whisker is a graphitic material formed by rolling up an atomic layer of graphite into a scroll, and was discovered in 1960. Usually the graphite whiskers are produced by DC arc discharge under high gas pressures (92 atm). These whiskers are up to ~3 cm long and 1~5 μm in diameter and are found to exhibit great crystalline perfection, high electrical conductivity, and high elastic modulus. Carbon whisk structure scheme is given in Figure 1.3 (a).

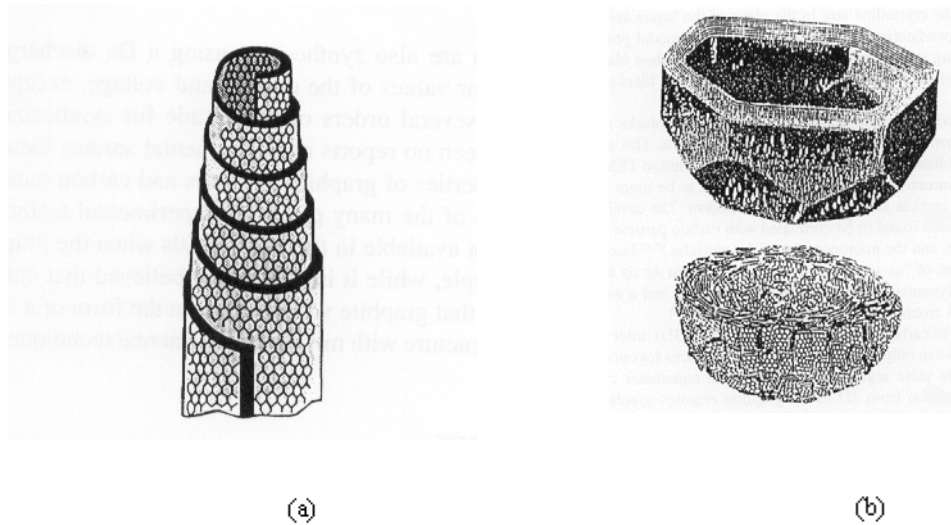


Figure 1.3 (a) Carbon Whiskers⁵ and (b) Carbon Black.^{6,7}

1.1.3 Carbon Black

Carbon blacks are fine carbon particles that are normally produced by dehydrogenation of hydrocarbon. Carbon blacks are widely used in industry as a filler to

modify the mechanical, electrical, and optical properties of the materials. Carbon blacks are composed of small graphite like layers, usually arranged concentrically. Carbon black particle scheme is given in Figure 1.3 (b).

1.1.4 Fullerenes and Carbon Nanotubes

The discovery of C_{60} fullerenes in 1985 by Kroto, Heath, O'Brien, Curl, and Smalley⁸ led to the discovery of carbon nanotubes by Iijima⁹ in 1991.

Carbon nanotubes can be seen as rolled graphene sheets closed at ends with hemispheres of fullerenes. According to the constituent carbon atom layers, carbon nanotubes can be classified as Single Wall Carbon Nanotubes, Double Wall Carbon Nanotubes, and Multi-Wall Carbon Nanotubes. Carbon nanotubes are synthesized by various methods, including the chemical vapor deposition (CVD), HiPCOTM and electric arc methods¹⁰.

1.1.5 Structure and Properties of Single Wall Carbon Nanotubes

The carbon nanotubes can be metallic or semi-conducting depending on their diameter and the helicity¹¹. The diameter and helicity of a SWNT can be represented by

$$C_h = na_1 + ma_2, \text{ or } (n,m), \quad (1.1)$$

where C_h is the chiral vector of the carbon nanotube, a_1 and a_2 are unit vectors in the two-dimensional hexagonal lattice, n and m are integers. The schematic of a two-dimensional graphene sheet illustrating lattice is shown in Figure 1.4.

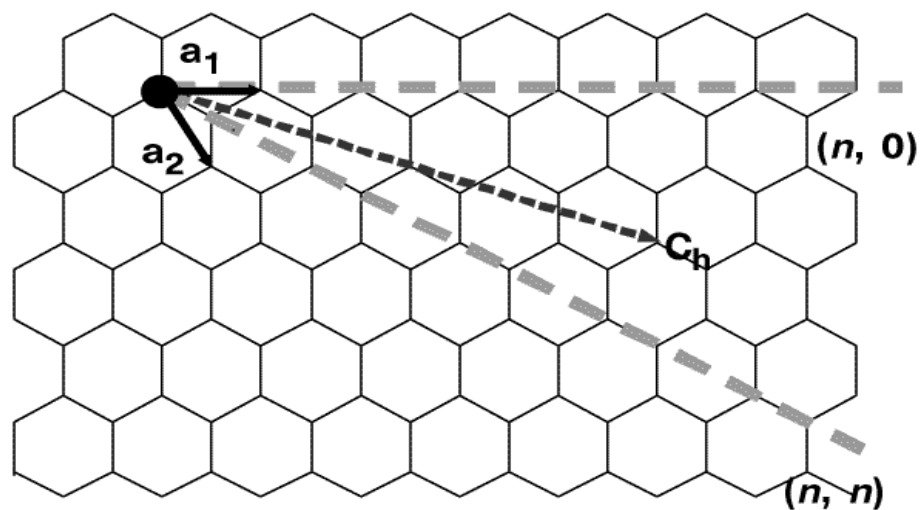


Figure 1.4 Schematic of a graphene sheet illustrating lattice vectors.¹¹

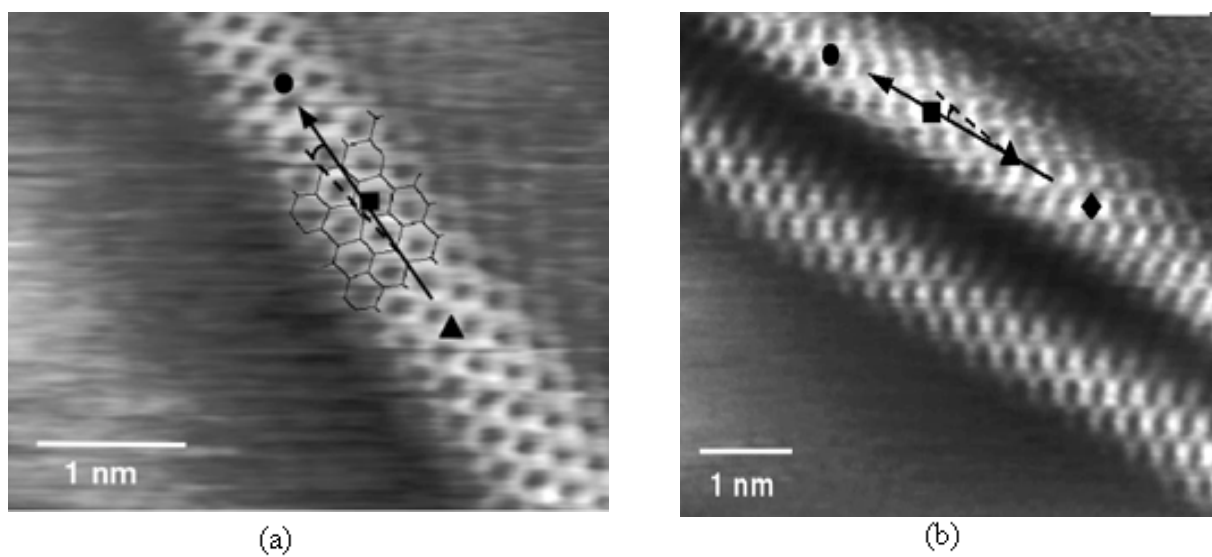


Figure 1.5 Atomic structure of SWNTs: (a) zigzag and (b) armchair.¹¹

When $n=m$, the SWNTs' structures are called armchair structure; when $m=0$, the SWNTs' structures are called zigzag structure. The TEM images of zigzag and armchair structures are given in Figure 1.5.

Generally if $n - m$ can be divided by 3, SWNTs are metallic, otherwise they are semi-conducting.¹² The conduction occurs normally in armchair tubes where conduction bands always cross each other at the Fermi Energy. In most helical tubes, the one dimensional band structure shows an opening of the gap at the Fermi energy, leading to semi-conducting properties. As the diameter of the tubes increases, the band gap tends to decrease until it becomes close to the zero gap.

Some vibrational modes in nanotubes can be excited by Raman spectroscopy, and the position of breathing modes in the Raman spectra shifts with the diameter of the tubes, this can be used to measure the distribution of nanotube diameters.¹³

The SWNTs usually self organized into ropes of 10~500 SWNTs in a two dimensional triangular lattice. Ropes from different SWNTs of different diameters have different lattice parameters, but the distance between the carbon nanotube walls are always constant, which is equal to 0.34 nm.¹⁴ The TEM images of SWNT ropes are given in Figure 1.6.

The mechanical properties of SWNT ropes are very important in our research and are listed in Table 1.1. The other physical properties of SWNT are summarized in Table 1.2.

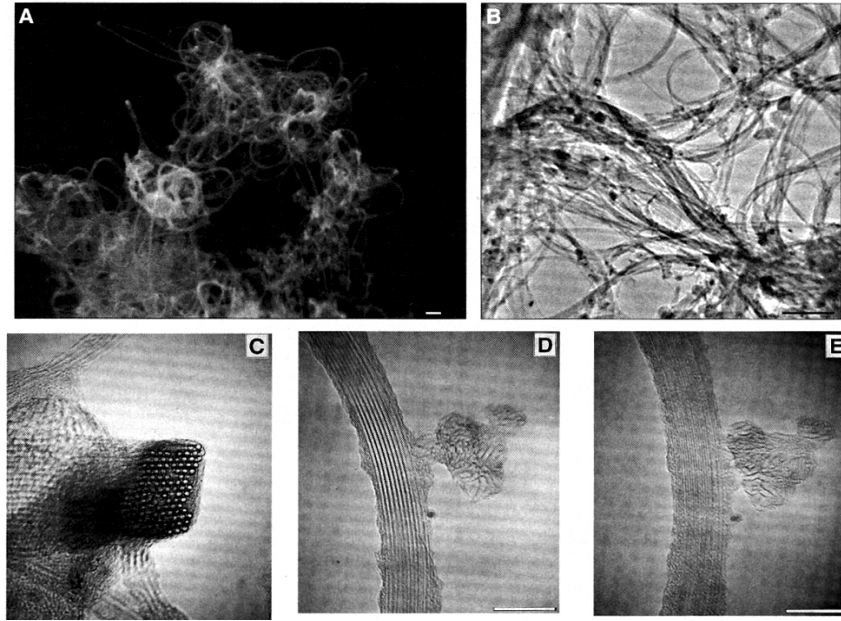


Figure 1.6 Rope Assembly of SWNTs.¹⁴

Table 1.1 Mechanical Properties of SWNT Ropes

Properties	Theoretical Value	Experimental Value
E_1	$\sim 1 \text{ TPa}^{15}$	$\sim 800 \text{ GPa}^{16,17}$
E_2	15 GPa	
G_{12}	19.5 GPa	1.0 GPa(rope diameter $\sim 20 \text{ nm}$) ^{21,22} 6.0 GPa (rope diameter $< 4.5 \text{ nm}$) ²²
σ		52 GPa ¹⁶

In Table 1.1, E_1 is the Young's modulus along the SWNT rope axis, E_2 is the Young's modulus along the SWNT rope's radial directions, G_{12} is the shearing modulus in the plane perpendicular to the rope axis, σ is the breakage strength along the SWNT rope axis.

Table 1.2 Physical Properties of SWNTs

Average Diameter of SWNTs	1.2 -1.4 nm ¹⁸
Lattice	Bundles of Ropes of Nanotubes Triangular Lattice (2D) ¹⁹
Lattice Constant	17 Å ¹³
Optical Properties (Fundamental Gap) ²⁰	
For (n, m); n-m is divisible by 3 [Metallic]	0 eV
For (n, m); n-m is not divisible by 3 [Semi-Conducting]	~ 0.5 eV
Electrical Transport Properties	
Conductance Quantization	(12.9 kΩ) ⁻¹
Resistivity	10 ⁻⁴ Ωcm
Maximum Current Density	10 ¹³ A/m ²
Thermal Transport Properties ²¹	
Thermal Conductivity	~ 2000 W/m/K
Phonon Mean Free Path	~ 100 nm
Relaxation Time	~ 10 ⁻¹¹ s
Elastic Behavior ²²	
Young's Modulus (SWNT)	~ 1 TPa
Young's Modulus (MWNT)	1.28 TPa
Maximum Tensile Strength	~ 100 GPa

1.1.6 Potential Applications of SWNTs

1.1.6.1 High Performance Composite Material

The extraordinary mechanical properties and high aspect ratio of SWNTs make them excellent candidates for high performance composite fillers. The mechanical properties of polymers can be greatly enhanced by the addition of carbon nanotubes. Experiments indicate that there is good load transfer and interface between SWNTs and polymers.²³ Increased thermal stability²⁴, glass transition temperature and storage modulus with the addition of carbon nanotubes in various polymer matrices have been reported.²⁵

1.1.6.2 AFM Probe

The resolution of AFM is determined largely by the size and shape of the probe tips. The current commercially available tips place significant constraints on potential lateral resolution. However, due to the high flexibility and small diameter, SWNTs can be the ideal choice for AFM tips.^{26, 27}

1.1.6.3 Super-capacitor

SWNT/Polymer composites have high porosity, specific surface area and electrical conductivity. Therefore, SWNTs are promising candidates for producing high energy storage super-capacitors.^{28, 29}

1.2 Polyacrylonitrile

Acrylonitrile ($\text{CH}_2\text{CH}(\text{CN})$) polymerizes to polyacrylonitrile (PAN, $-\text{[CH}_2\text{-CH}(\text{CN})\text{-]}_n\text{-}$). PAN is usually synthesized using free radical polymerization. Usually they are copolymers of acrylonitrile and methyl acrylate, or acrylonitrile and methyl methacrylate. PAN has a melting point of about 319°C , but it also decomposes at this temperature. So PAN is not suitable for melt spinning. PAN is soluble in N,N-Dimethyl Formamide (DMF), and this solution can be used in wet spinning to produce fibers.³⁰ Polyacrylonitrile fibers are used to make knitted clothing, like socks and sweaters, as well as outdoor products, awnings, sails for yachts, hot gas filtration systems, and even fiber reinforced concrete.³¹

Polyacrylonitrile is a major precursor for the production of carbon fibers, which is widely used in engineering composites in aerospace and automobile industry.³² The modulus of final carbon fiber is proportional to the modulus of the PAN precursor fiber.³³

1.3 Composite Fiber

High performance fiber is in great demand in industry for various applications because they possess high modulus, high strength, low density, as well as other electrical or thermal properties. SWNTs are excellent candidates for producing composite fibers due to the unique combination of properties of SWNTs, such as high modulus, high tensile strength, large aspect ratio, flexibility and resilience, chemical stability, etc. Good load transfer between polymer and SWNTs has been reported.^{34 35}

Carbon black has been used in reinforcing rubbers, however, we have not found any report about the application of carbon black, graphite or clay in reinforcing PAN fibers. It

is very promising that we can combine SWNTs with another polymer, say polyacrylonitrile, to produce a new composite material, which has the excellent properties of these two individual components. SWNT/PAN composite fibers have potential applications in structural composites, electrical shielding device, flat panel display, and heat dissipation management, optical devices, etc. It is predicted that the automobile and aerospace industry will increase their consumption of composite fibers for the component materials.

1.4 SWNT Functionalization

Dispersion and exfoliation of SWNTs, interaction between SWNTs and polymer are currently the major issues in producing SWNT/polymer composite fiber. People are investigating various methods, including mechanical processing, e.g. compounding, shear stirring, sonication, as well as chemical functionalization.³⁶

Nitric acid is used in the purification of SWNTs.^{37, 38} Nitric acid treatment can be used to remove impurities as well as amorphous carbon metal catalyst from SWNTs. TEM images taken from materials reacted in the HNO₃ solution for 24 hours and de-intercalated by heating under vacuum indicate that there is partial exfoliation.³⁹ Nitric acid may also oxidize SWNTs and produce carboxyl groups, which in turn may increase the interaction between polymer and SWNTs. Therefore, we chose nitric acid to treat SWNTs before they are mixed with PAN to spin into fibers and compare the fibers from non-acid SWNT/PAN. We chose 6M HNO₃/2 hours treatment, as it was found to be most efficient.⁴⁰

Benzonitrile functionalized SWNTs were synthesized by Prof. Jim Tour's group at Rice University. We spun fibers from these SWNTs and compared results with other experiments.

1.5 Objectives

We want to study the properties of SWNT/PAN composite fibers to:

- Search for an effective method to disperse SWNTs in PAN and to spin them into composite fiber.
- Investigate the property improvement effect of SWNT on the composite fiber.
- Investigate the effect of nitric acid treatment of SWNTs on the properties of SWNT/PAN composite fibers.
- Investigate the effect of benzonitrile functionalized SWNTs on the properties of SWNT/PAN composite fiber.

CHAPTER 2 EXPERIMENTAL

2.1 General Procedure

Single wall carbon nanotubes used in this study were produced from high pressure carbon monoxide (HiPCO™) Process at Rice University.^{41,42} These tubes were purified using nitric acid reflux process.⁴³ Based on the thermo-gravimetric analysis in the air, the purified tubes have 7 wt% residues at 800 °C.

Dimethyl Formamide (DMF) and polyacrylonitrile –co-methylacrylate [P(AN/MA)] copolymer were obtained from Sigma-Aldrich and were used as received. The P(AN/MA) copolymer ratio is 90:10 and the polymer molecular weight is ~ 100,000 g/mol.

According to the experimental requirements, SWNTs were either vacuum dried at 100 °C for 5 hours or subjected to special treatment (e.g. nitric acid treatments) before they are mixed with DMF solvent, otherwise the water contained in the SWNTs may reduce the dispersability of SWNTs in DMF/PAN mixture in the later steps. After the SWNTs are mixed with DMF, the solution is sonicated at room temperature for two hours using a bath sonicator (Branson B-22-4 bath sonicator).

During the sonication process, the SWNT/DMF mixture was stirred every half an hour with a bio-homogenizer (Biospec Products Inc. M133/1281-0) for a few minutes each time. The solution was then transferred to a glass flask and the excess solvent was boiled off to obtain the required final SWNT/DMF volume to which P(AN/MA) copolymer was added and dissolved while stirring at room temperature until a homogeneous dope is obtained.

The dope is finally used for fiber spinning using the dry-jet wet spinning technique. Sonication of SWNT bundle samples in solution may also yield isolated SWNTs, but the heavy sonication method is less appropriate for single nanotubes, since nanotube defects and nanotube fracture occurs through the sonication process itself, and small bundles often persist after sonication. Nanotubes enclosed by SDS surfactant can help tubes separate by sonication.⁴⁴ However, the presence of the SDS micelles should modify the basic properties of the nanotubes to some extent. Thus in our experiment, no surfactant was used. SWNT/PAN dope preparation setup is shown in Figure 2.1



Figure 2.1 SWNT/PAN dope preparation setup.

2.2 Non-acid Treated SWNT/PAN Dope

In the non-acid treated SWNT/PAN case, SWNT/PAN/DMF dope was prepared as follows:

- 0.75 g of SWNTs were mixed with 200 ml DMF solvent and sonicated at room temperature for two hours, the SWNT/solvent mixture was stirred every half an hour with a bio-homogenizer for 3 minutes.

- 14.25 grams of P(AN/MA) copolymer was ground with pestle and added to the solution while stirring at 25 °C.
- After mixing, solution is stirred until excess solvent was evaporated to obtain a final SWNT/PAN/DMF solution of 100 ml. At this stage, it is very important to avoid uneven DMF evaporation because this will cause inhomogeneity in the solution.

The final dope is a solution of 100 ml of non-acid treated SWNT/PAN suspension (SWNT/PAN =5:95, solid content 15%). Under optical microscope, the dope is homogeneous, indicating that the SWNTs are evenly dispersed in the solution as shown in Figure 2.2.

2.3 Nitric Acid Treatment of SWNTs

We followed the steps described below to treat SWNTs with nitric acid:

- SWNTs is treated with 6M HNO₃ and sonicated for two hours at room temperature, then refluxed for two hours, the boiling temperature in about 120 °C.
- Under room temperature, wash SWNTs with distilled water and centrifuge to separate the solvent. Repeat these steps three times.
- Under room temperature, wash the SWNTs with DMF and centrifuge to separate the solvent. Repeat this step three times.
- Under room temperature, add DMF to the solid content to make a 100 ml SWNT/DMF solution.

2.4 Nitric Acid Treated SWNT/PAN Dope

7.6 grams of P(AN/MA) were ground using pestle and then gradually added to the DMF solution that containing 0.4 gram nitric acid treated SWNTs. The dispersion was stirred for about 16 hours at 25 °C until the excess DMF was evaporated. The final dope was about 50 ml of SWNT/PAN/DMF, in which solid content was 15 % and the ratio of SWNTs to P(AN/MA) was 5:95. The final dope is an optically homogeneous mixture of SWNTs, PAN and DMF.

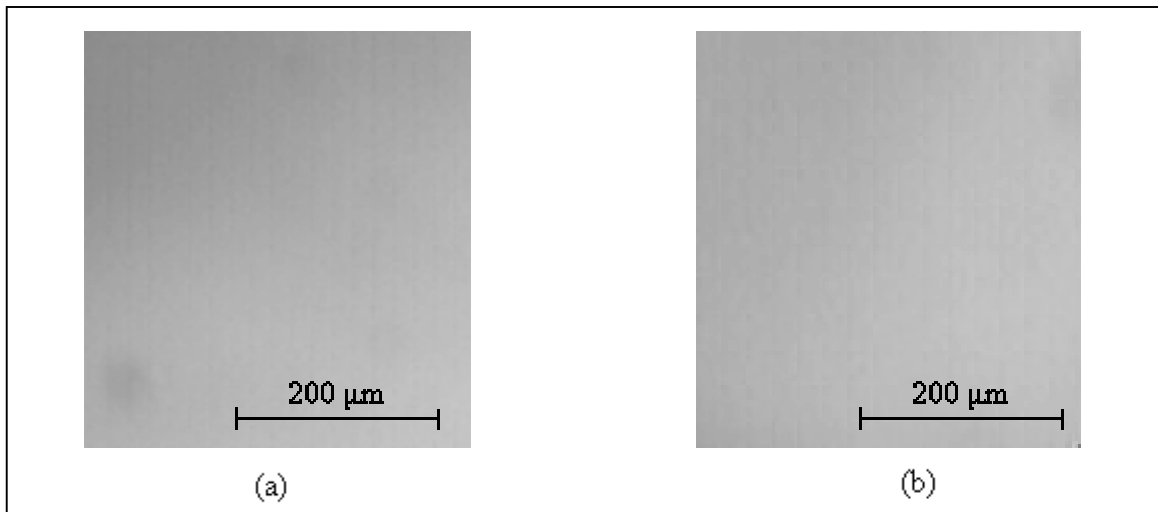


Figure 2.2 Optical Micrographs of (a) non-acid treated , (b) nitric acid treated SWNT/PAN dope.

2.5 SWNT/PAN Fiber Spinning

The dope was dry-jet wet spun on a laboratory-scale spinning machine manufactured by Bradford University Research Ltd, using a single-hole spinneret of 500 μm diameter. A 635 mesh (20 μm) stainless steel filter pack (from TWP Inc) was used in the spinning process. The dope temperature was maintained at 80 °C, and the air gap (distance between the spinneret orifice and the liquid surface in the first coagulation bath)

was about 5 cm. The spinning conditions for SWNT/PAN fibers and the spinning setup are shown in Table 2.1 and Figure 2.3, respectively. The non-acid treated and nitric acid treated SWNT/PAN composite fiber was spun using the same equipment and spinning conditions. The temperature and solvent concentration in baths I and II are chosen to insure good coagulation according previous report.

Table 2.1 Spinning conditions for SWNT/PAN composite fiber

Coagulation Bath I	
Composition	DMF: H ₂ O (ratio 60:40)
Temperature	25 °C
Take up Roller Speed	1.4 m/min
Coagulation Bath II	
Composition	DMF: H ₂ O (ratio 10:90)
Temperature	25 °C
Take up Roller Speed	1.4 m/min, Draw ratio $\lambda_1 = 1.0$
Coagulation Bath III	
Composition	DMF: H ₂ O (ratio 0:100)
Temperature	90 \pm 5 °C
Take up Roller Speed	7.9 m/min, draw ratio $\lambda_2 = 5.62$
Drying on a hot plate	
Hot plate temperature	120 °C
Wind Speed	8.0 m/min, draw ratio $\lambda_3 = 1.02$
Total Draw Ratio($\lambda_1 \lambda_2 \lambda_3$)	5.73

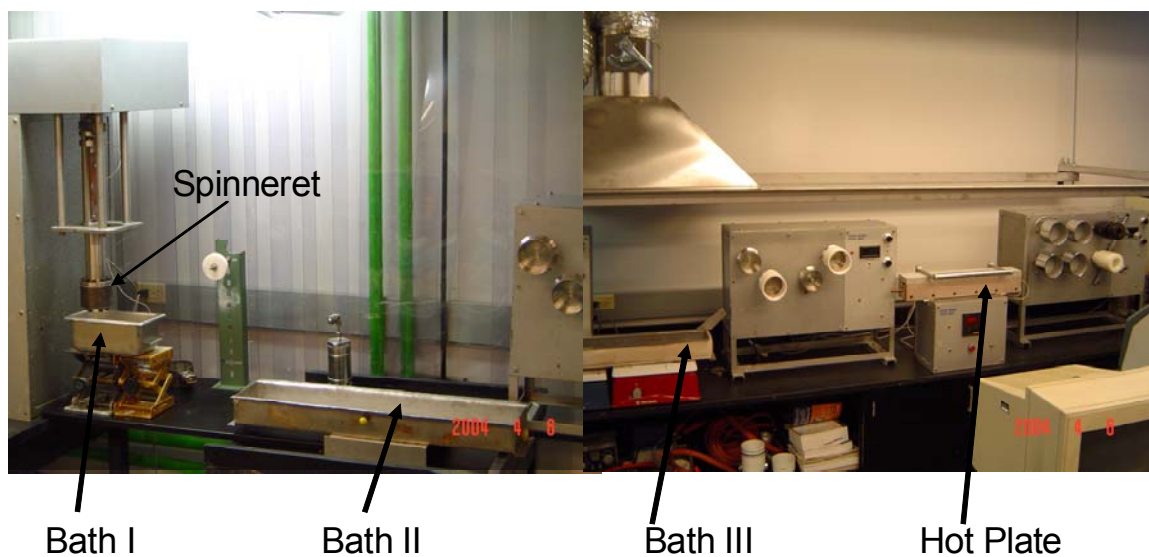


Figure 2.3 Fiber spinning setup.

2.6 Benzonitrile Functionalized SWNTs/PAN Composite Fiber

Prof. Jim Tour's research group at Rice University has affixed large addends (benzonitrile) onto the sidewalls of SWNTs to improve the SWNT solubility.⁴⁵ Here we try to investigate the reinforcement effect of these benzonitrile functionalized SWNTs.

2.6.1 Benzonitrile Functionalized SWNTs

There are two samples of benzonitrile functionalized SWNTs:

- JLH-II-085 is a sample prepared by SDS functionalization method which should consist mainly of functionalized individual SWNTs;
- JS-2-88 is a sample prepared by a solvent free method, which should consist mainly of functionalized SWNT Ropes.

The scheme of these two kinds of SWNT samples are shown in Figure 2.4.

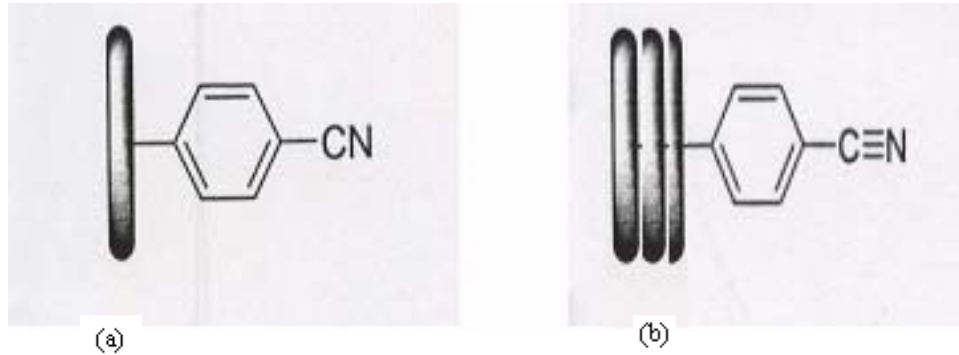


Figure 2.4 Functionalized SWNTs: (a) JLH-II-085 SWNTs and (b) Js-2-88 SWNTs.

2.6.2 PAN from Exlan Inc. (Japan)

For benzonitrile functionalized SWNT/PAN composite fiber, we used PAN powder from Exlan Company (Japan). Two kinds of PAN powders, Exlan_PAN_A and Exlan_PAN_B exhibit good solubility in DMF. The viscosity averaged molecular weight of these two types of PAN powders were determined using dilute solution viscometry. Viscosity data is plotted in Figure 2.5.

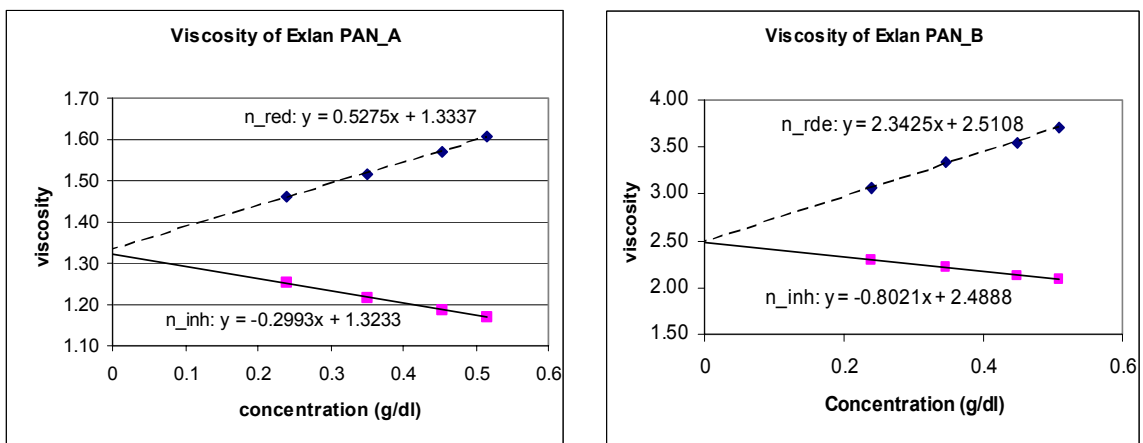


Figure 2.5 Viscosity data of Exlan PAN.

From viscosity data we obtained

$$[\eta]_A = 1.32 \text{ dl/g}, [\eta]_B = 2.49 \text{ dl/g}, \quad (2.1)$$

where $[\eta]_A$, $[\eta]_B$ are the intrinsic viscosities for Exlan_PAN_A and Exlan_PAN_B, respectively. According Mark-Houwink-Sakurada relationship,

$$[\eta] = KM^a, \quad (2.2)$$

where $[\eta]$ is the intrinsic viscosity of a polymer solution, K and a are constants which can be taken as $2.86 \cdot 10^{-4}$ and 0.7335 respectively for PAN/DMF solution⁴⁶, we can calculate viscosity averaged molecular weight for Exlan_PAN_A (M_{v_A}) as 99800 and that for Exlan_PAN_B (M_{v_B}) as 236000.

The FTIR spectra of these two types of PAN powders are given in Figures 2.6. The FTIR absorption peak assignments are listed in Tables 2.2 and 2.3. After IR match search, we decided that Exlan_PAN_A sample is poly(acrylonitrile-co-methylacrylate) copolymer, and Exlan_PAN_B is 100% polyacrylonitrile.

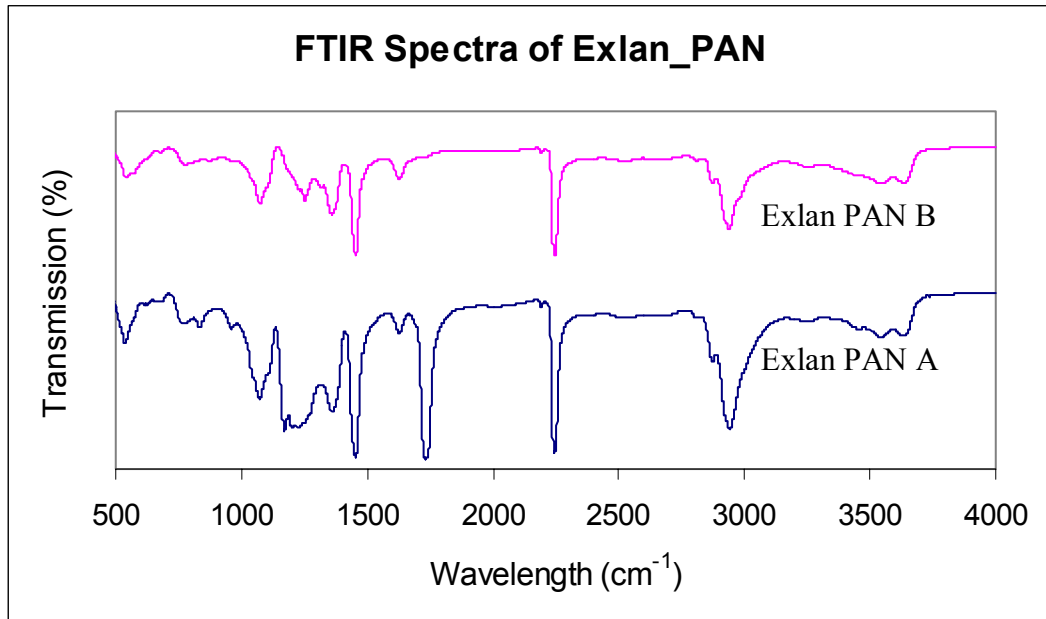


Figure 2.6 FTIR pattern of Exlan PAN sample powder.

Table 2.2 FTIR Absorption Peaks and Assignments for Exlan PAN

Peak Positions (cm ⁻¹)	Exlan PAN A	Exlan PAN B	Assignments
3544	√	√	N-H formed by partial hydrolysis
3250	√	√	OH of OH-COCH ₂ -C(=CH ₂)COOH
2941	√	√	C-H of -CH ₂ of in acrylonitrile
2873	√	√	C-H of -CH ₂ in acid
2244	√	√	-C≡N
2191	√	√	-C=N
1733	√		-C=O of -COOH
1626	√	√	-C=C
1454	√	√	C-H of -CH ₂ -
1360	√	√	C-H of acrylonitrile
1202	√		-C-CN
1171	√	√	C—CH ₃ , or C-CH ₂ -COOH
1072	√	√	C—CH ₃ , or C-CH ₂ -COOH
960	√		C—CH ₃ , or C-CH ₂ -COOH

2.6.3 Benzonitrile Functionalized SWNT/PAN Fiber Spinning

The dope preparation and fiber spinning procedures here are similar to the method described in Sections 2.1 to 2.5. The micrographs of these two dopes are given in Figure 2.7. The weight percentage of SWNTs in SWNT/PAN samples are 0.2%.

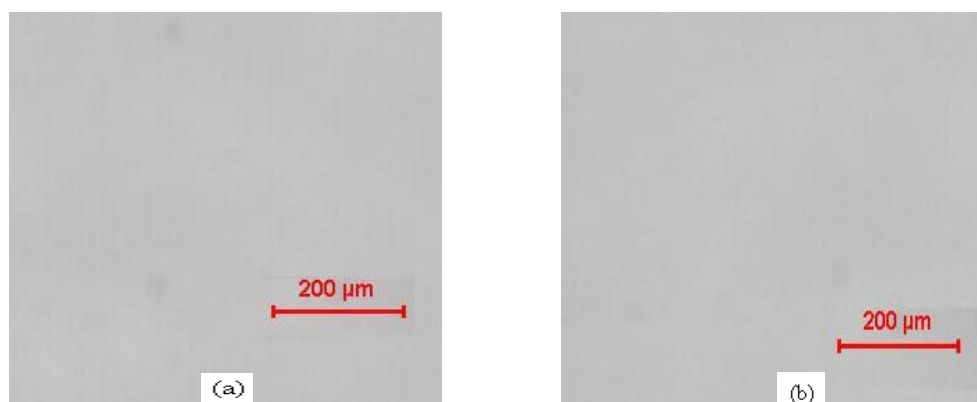


Figure 2.7 Optical micrographs of (a) JLH-II-085/PAN and (b) JS-2-88/PAN Dope.

CHAPTER 3 CHARACTERIZATION AND ANALYSIS

3.1 SWNT/PAN Composite Fiber

3.1.1 Geometric Properties

The Scanning Electron Micrographs of SWNT/PAN composite fibers is shown in Figure 3.1 We can see that SWNT/PAN fibers do not have circular cross-sections. This is due to the diffusion of DMF into the bath.

The average densities of the composite fibers were calculated from their weight fractions. Assuming the densities of PAN and nanotubes as 1.18 g/cm^3 and 1.3 g/cm^3 , we obtain density of 1.186 g/cm^3 for the SWNT/PAN (5:95 wt %) composite fibers.

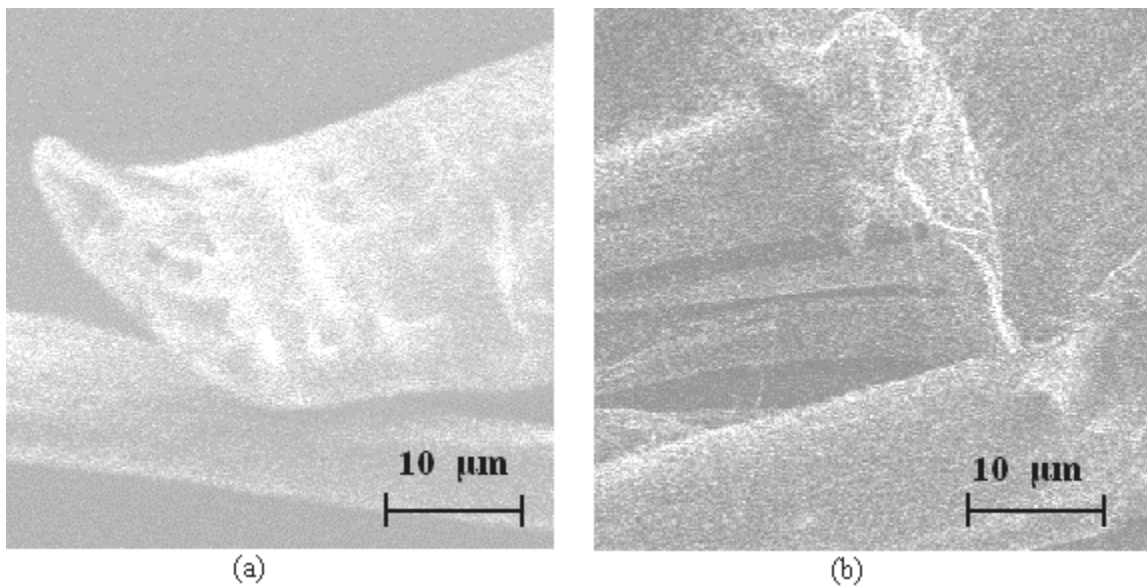


Figure 3.1 SEM images of (a) Non-acid treated SWNT/PAN, (b) Acid treated SWNT/PAN.

3.1.2 Tensile Test and Dynamic Mechanical Analysis

Control pure PAN fiber, non-acid treated SWNT/PAN composite and acid treated SWNT/PAN fibers were tested using Rheometrics Scientifics' Solids Analyzer. The gauge length was 25 mm and cross-head speed for the tensile tests was 10 mm/min. Ten samples were tested for each fiber. The results are shown in Table 3.1.

Table 3.1 Tensile properties of PAN and SWNT/PAN composite fibers

SWNT wt%	Tensile Modulus (GPa)	Tensile Strength (GPa)	Elongation at Break (%)
0 wt%	7.9 ± 0.2	0.23 ± 0.01	11.0 ± 0.08
5 wt% non-acid treated	13.1 ± 1.0	0.33 ± 0.04	8.6 ± 1.0
5 wt% acid treated	17.8 ± 1.3	0.45 ± 0.06	6.9 ± 2.0

We see that the tensile modulus of SWNT/PAN fiber showed great improvement as compared to pure PAN fiber, from 5.9 GPa to 13.0 GPa. The tensile strength increased from 0.23 GPa to 0.33 GPa.

After nitric acid treatment, composite fiber properties are further improved, modulus increased from 13.0 GPa to 17.8 GPa, tensile strength increased from 0.33 GPa to 0.45 GPa, a nearly 30% improvement compared to non nitric acid composite fibers.

The Dynamic Mechanical Analysis (DMA) was conducted at 10 Hz and 5°C/min on a Rheometrics Scientifics' Analyzer (RSA III). Results are shown in Figures 3.2, 3.3 and 3.4.

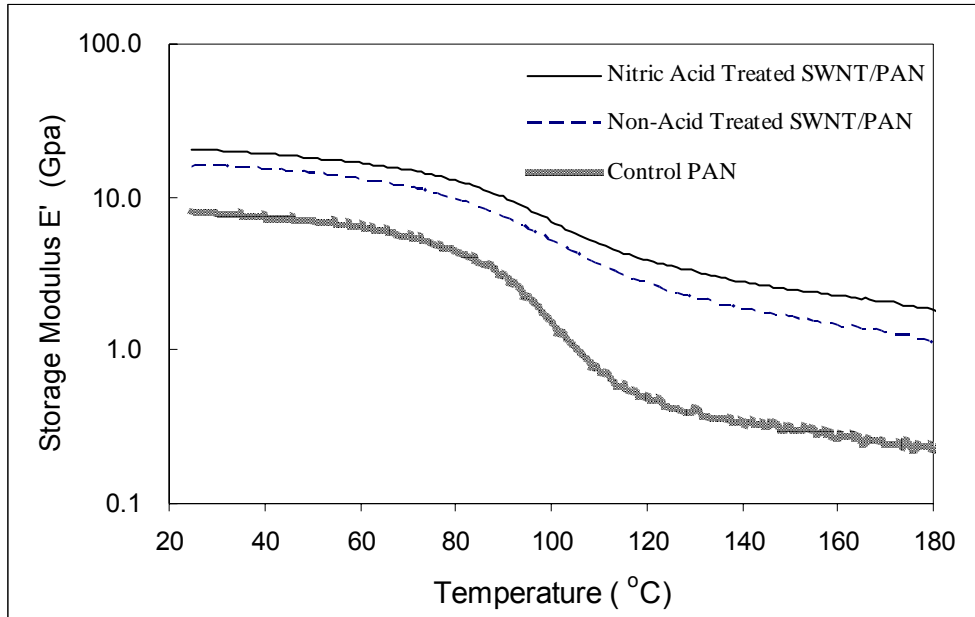


Figure 3.2 Storage moduli of control PAN and SWNT/PAN fibers.

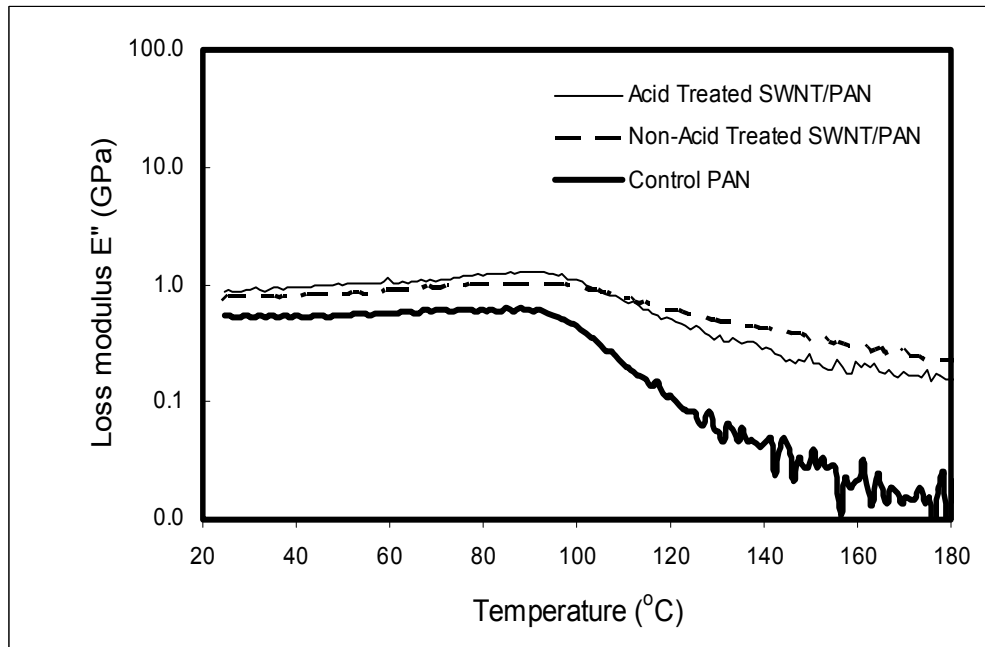


Figure 3.3 Loss moduli of control PAN and SWNT/PAN fibers.

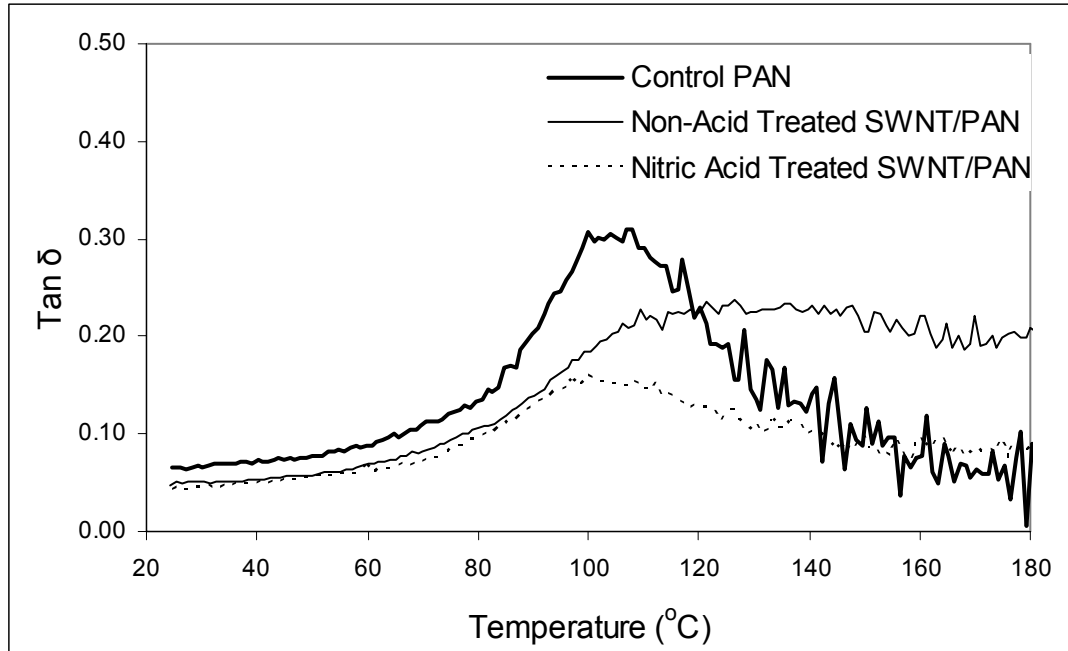


Figure 3.4 Loss tangent of control PAN and SWNT/PAN fibers.

Three samples were tested for each fiber; the results all show the similar curve. The DMA experiments showed the increased storage modulus property for SWNT/PAN composite fibers and further improvement for nitric acid treated SWNT/PAN fibers. The magnitude of loss tangent peak decreases correspondingly. The broadening of the loss tangent peak for non acid treated SWNT/PAN and the sharp downward slope of the loss tangent peak for nitric acid treated SWNT/PAN are evidences of SWNT/PAN interaction. The segmental movement of PAN chains is hindered by the SWNT/PAN interaction.

3.1.3 Thermo-Mechanical Analysis (Shrinkage)

The thermo-mechanical analysis (TMA) of SWNT/PAN fibers was determined using the TA Instruments thermo-mechanical analyzer (TMA 2940) at 0.2 MPa pre-stress. The heating rate was 10 °C/min. After heating from room temperature to 250 °C, the

sample was kept at 250 °C for half an hour. Three samples were tested for each fiber, and the test results are shown in Figure 3.5.

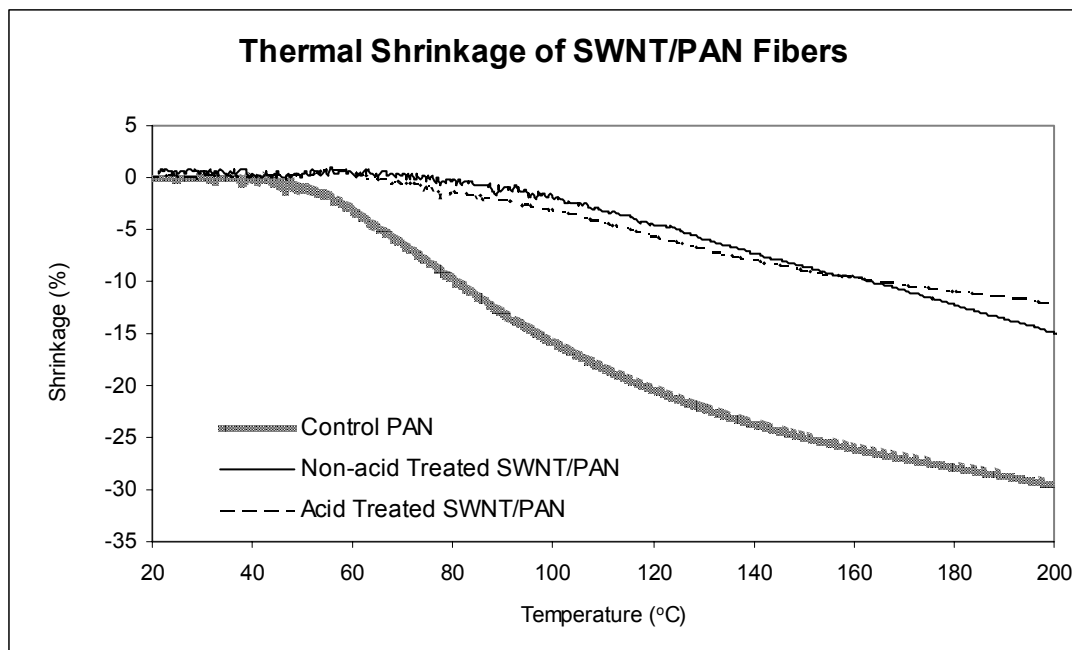


Figure 3.5 TMA of control PAN and SWNT/PAN fibers.

At 200 °C, shrinkage is about 14% for the non-acid treated SWNT/PAN fiber and 12% for the acid treated SWNT/PAN fiber; both values are less than half of the shrinkage in the control PAN fiber, which is about 30%. This result is consistent with Figure 3.6 which was obtained by previous researchers.⁴⁷ Because the shrinkage in PAN up to 200 °C is mostly entropic, this result indicates that the presence of SWNTs have a hindrance effect on the chain motion in the PAN molecule.

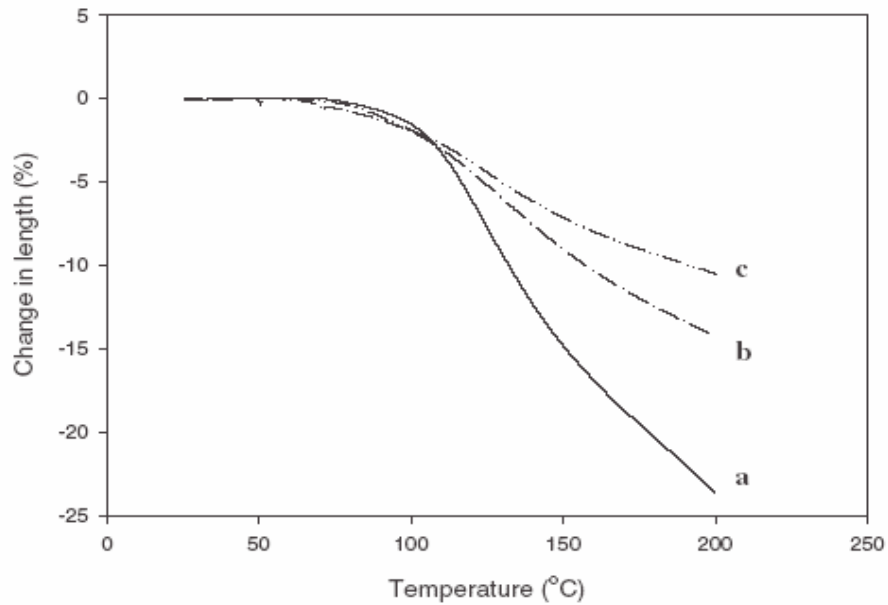


Figure 3.6 Thermal shrinkage in a) PAN, b) SWNT/PAN (5:95) and c) SWNT/PAN (10:90) composite fiber as a function of temperature.⁴⁷

3.1.4 Differential Scanning Calorimetry (DSC)

DSC experiments were carried out on TA Instrument Q-100 machine. DSC scans of second heating cycle at 10 °C/min are given in Figures 3.7. All samples show DSC T_g of about 95 °C.

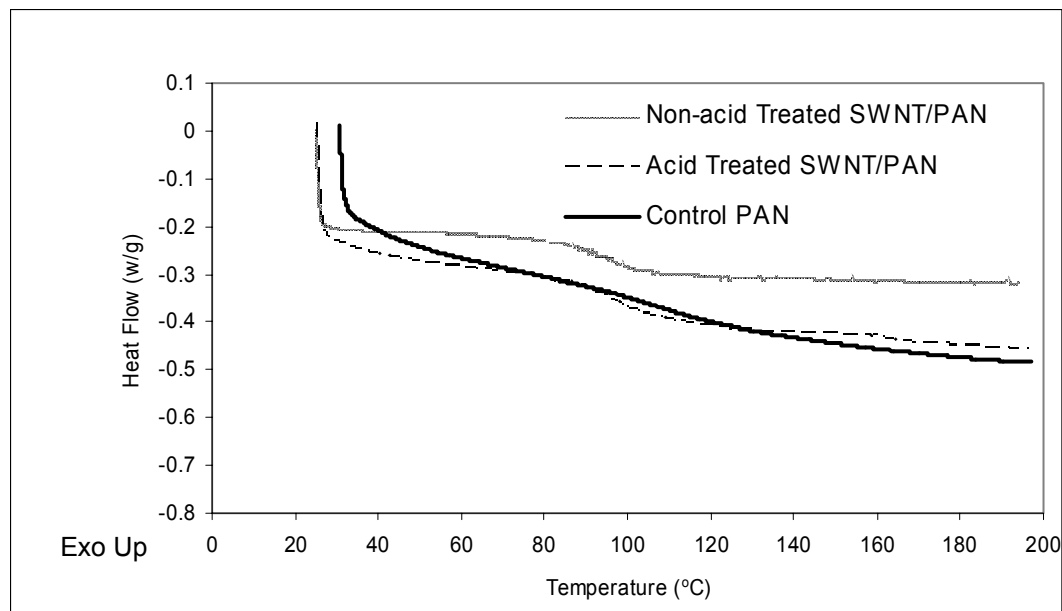


Figure 3.7 DSC of control PAN and SWNT/PAN fibers.

3.1.5 FTIR Spectra

The spun fibers were dissolved in DMF and then mixed with KBr powder. The FTIR spectra were collected on a Perkin Elmer FTIR spectrometer. A typical result is shown in Figure 3.8.

Comparison of the above FTIR spectra suggests that there is no significant difference between the non-acid treated SWNT/PAN and nitric acid treated SWNT/PAN. This is because even though nitric acid has introduced some -C=O or -COOH groups onto the SWNTs, the signal from these groups is perhaps too weak to be observed in the composite fiber.

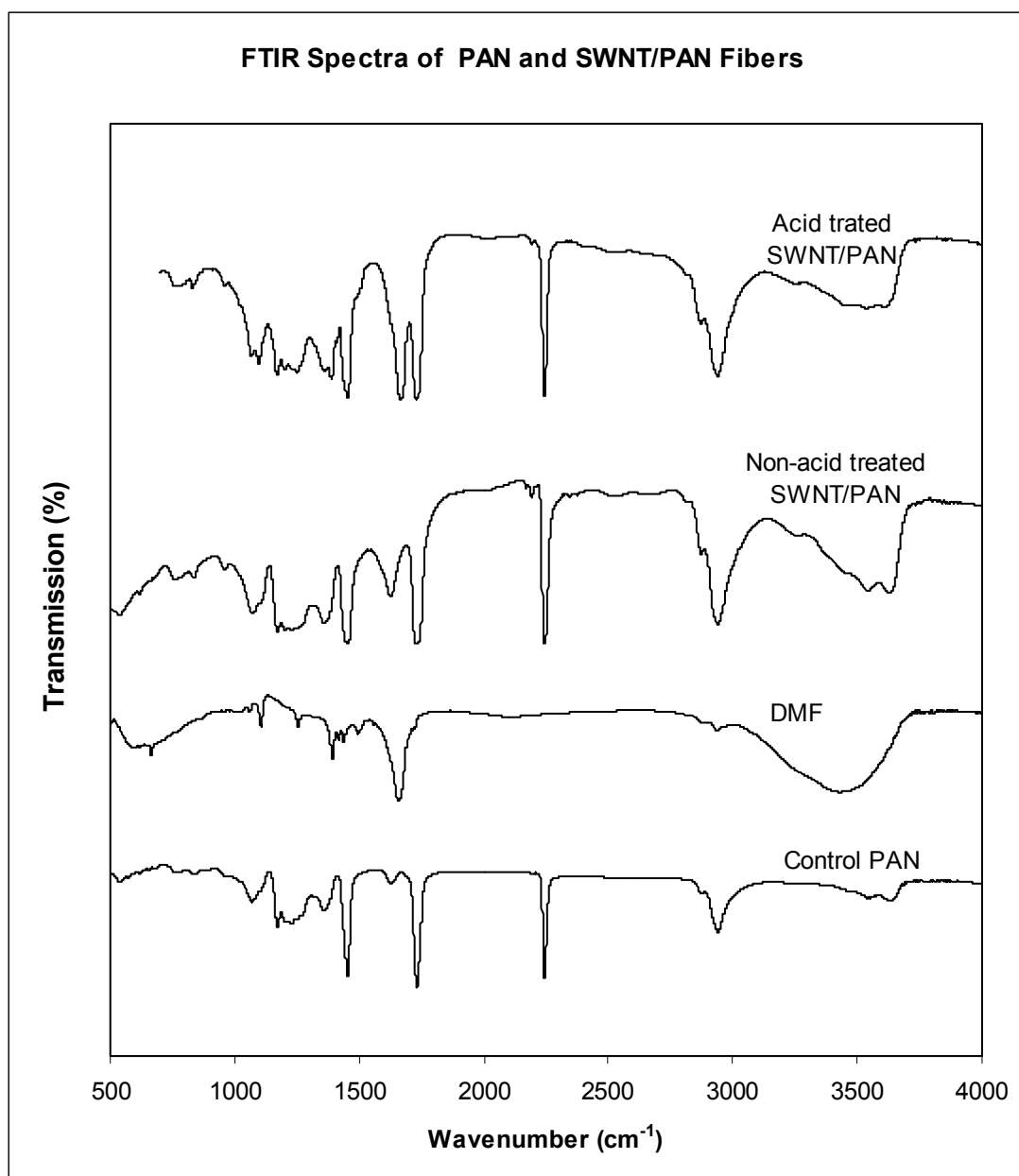


Figure 3.8 FTIR spectra of PAN and PAN fibers.

3.1.6 Raman Spectra

Usually Raman spectra only involve phonons explicitly, being independent of the electronic structure of the material and the laser energy used to excite the Raman spectra. Furthermore, the usual Raman scattering signal is weak. However, the scattering efficiency becomes larger when the laser energy matches the energy between optically allowed electronic transitions in the material, and this intensity enhancement process is called resonance Raman scattering⁴⁸. The resonance Raman intensity depends on the density of electronic states (DOS) available for the optical transitions, and this property is very important for one-dimensional (1D) systems. The peaks below 500 cm^{-1} are the RBMs from the resonant SWNTs.

The Raman tangential mode is observed at $1582\sim 1596\text{ cm}^{-1}$, and is called the G mode. The two most intense G peaks are labeled G^+ , for atomic displacements along the tube axis, and G^- , for modes with atomic displacement along the circumferential direction. The lowering of the frequency for the G^- mode is caused by the curvature of the nanotube which softens the tangential vibration in the circumferential direction⁴⁷. The schematics for RBM and G band vibration of SWNTs are given in Figure 3.9.

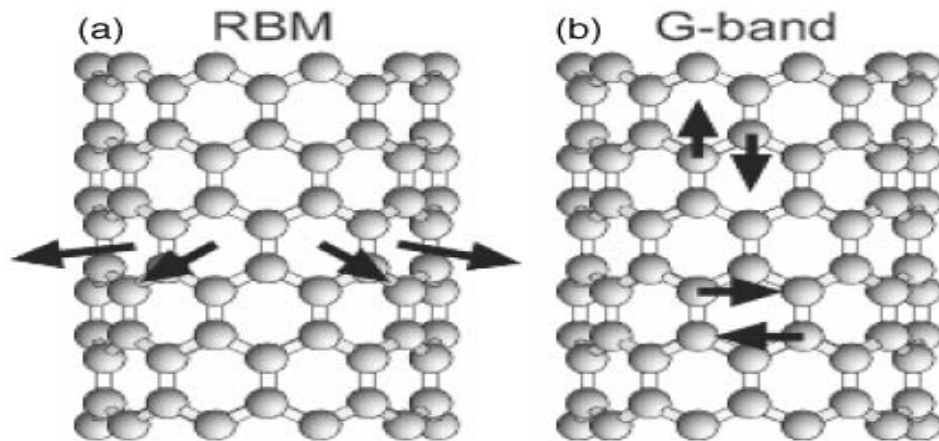


Figure 3.9 SWNT's atomic vibrations for (a) the RBM and (b) the G band modes.⁴⁹

When Raman spectra of SWNT bundle samples are taken, only those SWNTs with E_{11} in resonance with the laser excitation energy E_{laser} will contribute strongly to the spectrum.

The polarized Raman spectra was collected in the back scattering geometry using a Holoprobe Research 785 Raman Microscope made by Kaiser Optical System, Inc. with a laser wavelength of 785 nm. Measurements were made using a back scattering configuration when the angle φ between the fibers and the polarization direction of the exciting laser source was varied from 0 to 90 degrees. At each angle, the spectra were collected in a VV configuration, where the polarizer and the analyzer are parallel to each other. The Raman spectra patterns when fibers are at 0° to the polarizer are given in Figure 3.10.

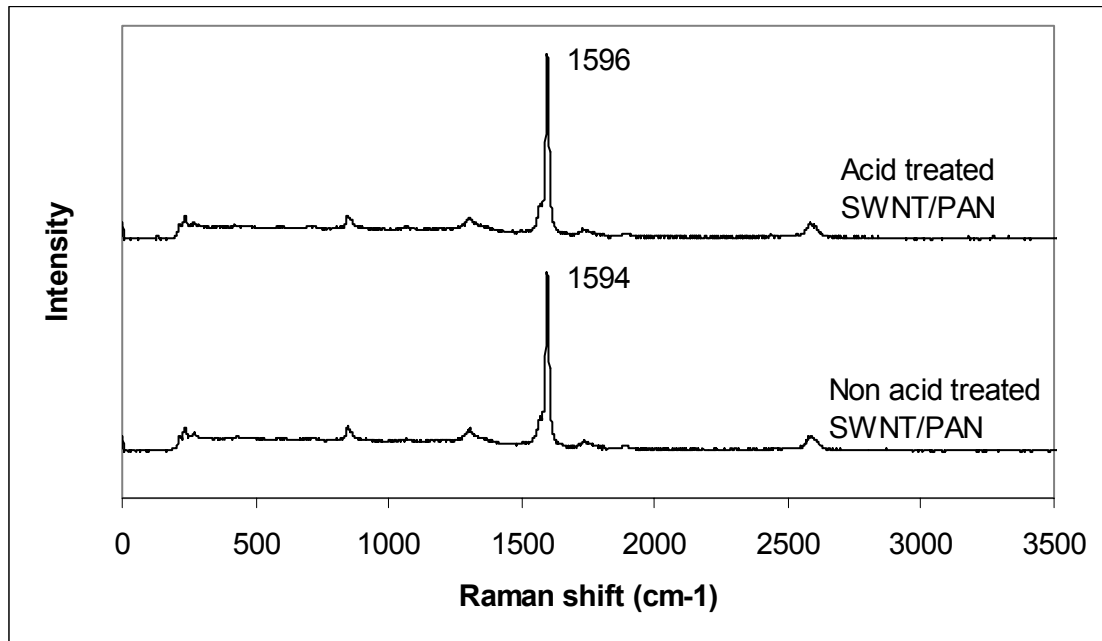


Figure 3.10 Raman spectra of SWNT/PAN fibers.

By comparing of the G band and RBM band position for non-acid treated and acid treated SWNT/PAN, we have observed that the Raman spectra remained unchanged for the most part, indicating that the SWNTs maintain their nanotube structure after our nitric acid treatment. Therefore the SWNTs can still keep their extraordinary properties in reinforcements. We have also noticed a small shift ($1\sim 3\text{ cm}^{-1}$) of the G band. This is in agreement with what was observed previously.^{50, 51} This indicates that the electronic structure of SWNTs did change due to the nitric acid treatment.

We change the angle φ between the fiber and the polarizer from 0° to 90° , and the corresponding peak value $I_{vv}(\varphi)$ of the G band are given in Table 3.2. The $I_{vv}(\varphi)$ values in this table will be used to calculate the Herman's orientation factor of SWNTs in Section 3.2.

Table 3.2 The G band peak value $I_{vv}(\varphi)$ of SWNT/Fibers

φ angle	0°	5°	10°	20°	30°	45°	60°	85°	90°
$I_{vv}(\varphi)$ for non-acid treated SWNT/PAN	3291	2980	2898	2333	1602	529	118	82	80
$I_{vv}(\varphi)$ for Acid treated SWNT/PAN	3660	2658	1991	1180	689	376	201	128	89

3.1.7 Wide Angle X-ray Diffraction Pattern (WAXD)

Wide angle X-ray diffraction (WAXD) patterns were collected for various fibers using x-ray source of wavelength 1.5406 \AA . The WAXD patterns are shown in Figure

3.11. The corresponding equatorial and azimuthal scans are shown in Figures 3.12 and 3.13. In these figures, 2θ is the Bragg angle and χ is the azimuthal angle of the WAXD pattern.

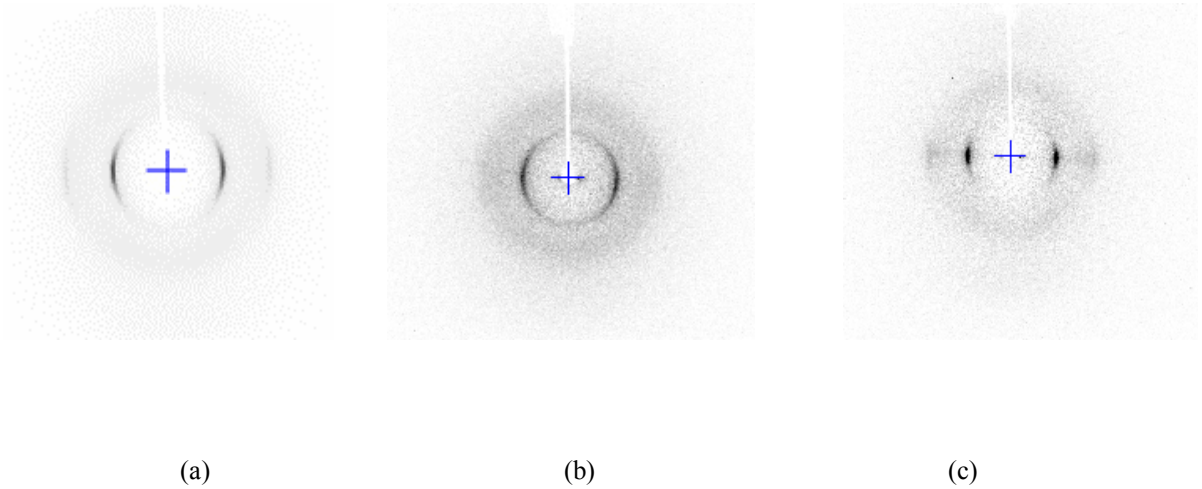


Figure 3.11 WAXD patterns of (a) control PAN, (b) non-acid treated SWNT/PAN and (c) acid treated SWNT/PAN fibers.

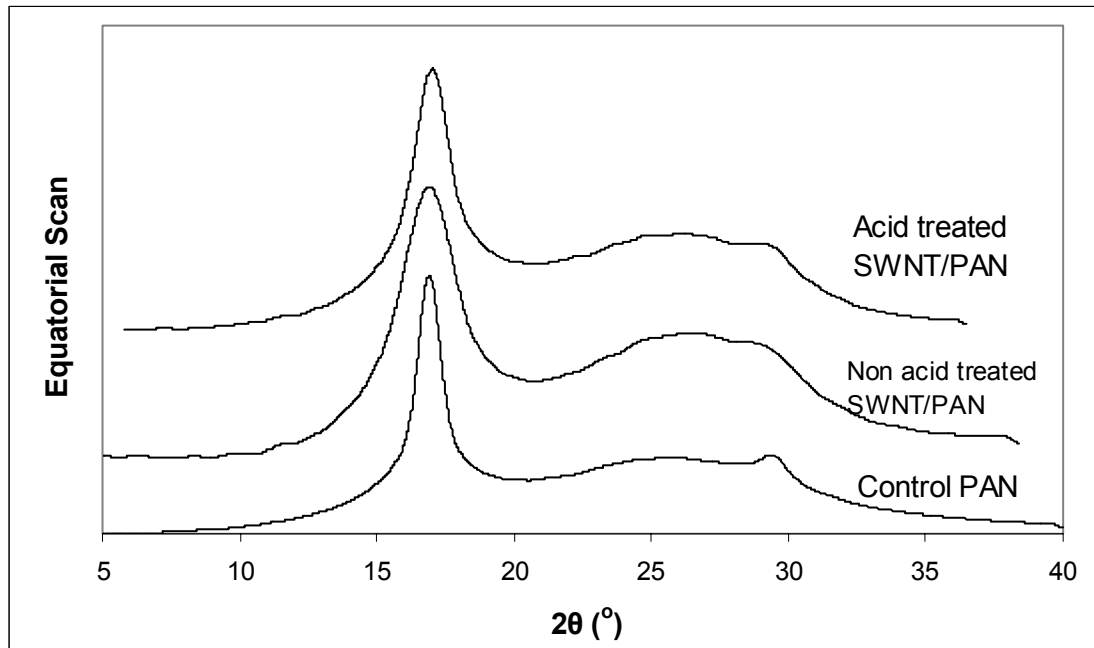


Figure 3.12 Equatorial WAXD scan of SWNT/PAN fibers.

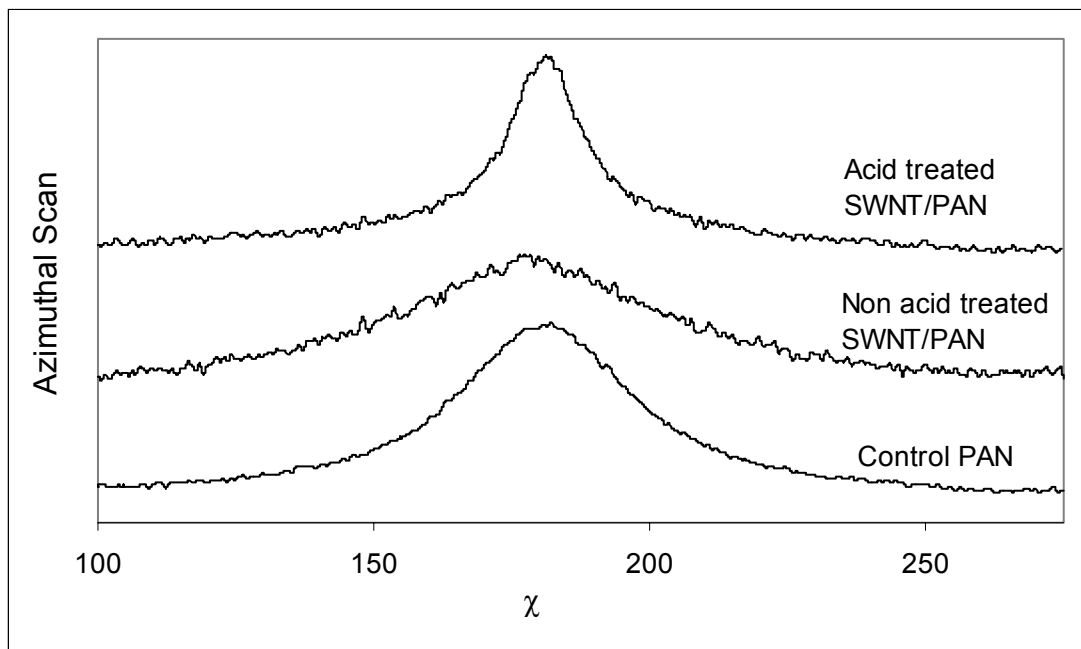


Figure 3.13 Azimuthal WAXD scan of SWNT/PAN fibers.

Table 3.3 PAN lattice data of control PAN and SWNT/PAN fibers

	Plane (10)			
	2Θ	d-spacing (Å)	FWHM	Crystal Size (Å)
Control PAN	16.97°	5.22	1.5°	53
Non-Acid Treated SWNT/PAN	17.14°	5.17	2.8°	29
Nitric Acid Treated SWNT/PAN	17.25°	5.14	2.9°	28

According to X. D. Liu and W. Ruland⁵², the positions of the sharp reflections correspond to the indices (10), and the calculated PAN lattice data are given in Table 3.3. These data are consistent with those reported in previous studies.^{53,54} We noticed that composite fibers have much smaller crystal size than control PAN fiber, this is because SWNTs reduced mobility of PAN chains, thereby hindering the crystal formation.

3.2 SWNT/PAN Composite Fiber Orientation

3.2.1 SWNTs Orientation

The Raman spectroscopy is an ideal characterization technique for the study of SWNT orientation in a SWNT/PAN composite fiber⁵⁵. The tangential mode of the SWNT Raman spectra of the SWNT/PAN composite fiber in the VV configuration decreases in intensity with increasing angle between the fiber axis and the polarization direction of the polarizer, indicating SWNT alignment in the composite fiber. We can utilize this phenomenon to quantify SWNT orientation in the fiber.

Suppose the orientation distribution function $F(\theta)$ of the SWNTs in the fiber is a Gaussian function⁵⁶,

$$F(\theta) = \exp\left(-\left(\frac{\theta}{w}\right)^2 \ln 16\right), \quad (3.1)$$

where θ is the angle between an individual SWNT and the fiber axis, $F(\theta)$ is the orientation distribution function, and w is the full width at half maximum of the orientation distribution function $F(\theta)$.

Theoretically, in the VV configuration where polarizer direction is parallel to the analyzer's direction, the intensity of G band when fiber is at different angle with respect to the polarizer's direction is given by,

$$I_{vv}(\varphi) = K \int_{-\pi/2}^{\pi/2} I_R(e_{s//}, \theta, \varphi) d\theta, \text{ and} \quad (3.2)$$

$$I_R(e_{s//}, \theta, \varphi) = \cos^4(\theta + \varphi) \alpha_{zz}^2 F(\theta), \quad (3.3)$$

where φ is the angle between the fiber and the polarizer, $I_{vv}(\varphi)$ is the G band peak intensity when fiber is at φ with the polarizer, K is proportional constant, $I_R(e_{s//}, \theta, \varphi)$ is the scattering light intensity of an individual SWNT, $e_{s//}$ is scattering coefficient, and α_{zz} is the polarizability in zz direction of an individual SWNT when the SWNT axis is parallel to the polarization direction of the incident light.

Hence, $I_{vv}(\varphi)$ is given by

$$I_{vv}(\varphi) = \int_{-\pi/2}^{\pi/2} \cos^4(\theta + \varphi) \alpha_{zz}^2 \exp\left(-\left(\frac{\theta}{w}\right)^2 \text{Ln}16\right) d\theta. \quad (3.4)$$

The optimum full width at half maximum, w , can be determined such that the theoretical value of $I_{vv}(\varphi)$ is close to the experimental Raman spectra value in Table 3.2. We used the least squares method in calculating w .

After w is obtained, the SWNT orientation function is determined and then the average value of $\cos^2\theta$ can be calculated as

$$\langle \cos^2\theta \rangle = \frac{\int_{-\pi/2}^{\pi/2} F(\theta) \cos^2\theta d\theta}{\int_{-\pi/2}^{\pi/2} F(\theta) d\theta}, \quad (3.5)$$

where $\langle \cos^2\theta \rangle$ is the average value of $\cos^2\theta$. Then the Herman's orientation factor f can be given by

$$f = \frac{3 \langle \cos^2\theta \rangle - 1}{2}. \quad (3.6)$$

Using the Matlab program in Appendix A, the Herman's orientation factor for the non-acid treated SWNT/PAN and the acid treated SWNT/PAN were calculated as 0.982 and 0.984, respectively.

3.2.2 PAN Molecule Orientation

The orientation of PAN molecules can be determined from the azimuthal integration of the WAXD pattern using the formula

$$\langle \cos^2 \varphi_{z,hkl} \rangle = \frac{\int \cos^2 \varphi_{z,hkl} I(\varphi_{z,hkl}) d\varphi_{z,hkl}}{\int \sin \varphi_{z,hkl} I(\varphi_{z,hkl}) d\varphi_{z,hkl}}. \quad (3.7)$$

where $\varphi_{z,hkl}$ is the angle between crystal plane hkl and z axis, and $\langle \cos^2 \varphi_{z,hkl} \rangle$ is the average value of $\cos^2 \varphi_{z,hkl}$. The orientation factor along the fiber axis were estimated to be 0.58, 0.54 and 0.60 for the control PAN, non acid treated SWNT/PAN and acid treated SWNT/PAN respectively.

3.3 SWNT/PAN Fiber Modulus

According to continuum mechanics⁵⁷, if an anisotropic material is subjected to a load at an angle of θ to a certain x axis, then the effective modulus of the material along the loading direction is given by

$$\frac{1}{\langle E_x \rangle} = \frac{1}{E_1} \langle \cos^4 \theta \rangle + \frac{1}{E_2} \langle \sin^4 \theta \rangle + \left(\frac{1}{G_{12}} - \frac{2\nu_{12}}{E_1} \right) \langle \sin^2 \theta \cos^2 \theta \rangle, \quad (3.8)$$

where $\langle E_x \rangle$ is the effective tensile modulus of the material along the loading direction, θ is the angle between the loading direction and x axis, E_1 is the modulus along the x axis, E_2 is the modulus along the y axis, G_{12} is the shear modulus of plane perpendicular to x axis, and ν_{12} is the Poisson's ratio.

Therefore, if given the Herman's orientation factor, f , of any component in a composite fiber, we can calculate its $\langle \cos^4\theta \rangle$, $\langle \sin^4\theta \rangle$ and its effective modulus in the composite fiber. Since SWNT/PAN composite fibers are anisotropic materials made up of SWNTs and PAN, we should first calculate the effective modulus of PAN and SWNTs. For PAN, the Herman's orientation factor, f , is determined from its WAXD data. The modulus of PAN at perfect orientation can be estimated using the experimental modulus of PAN and the respective Herman's orientation function. For SWNTs, since the SWNTs mainly exist in the form of bundles in composite fibers, we should consider the modulus of SWNT ropes. The Herman's orientation factor, f , of SWNT ropes is determined from the fiber's Raman spectra data, and their mechanical properties are given in Table 3.4.

Table 3.4 The mechanical properties of SWNT ropes⁵⁸

E_1	640 GPa
E_2	12 GPa
ν_{12}	0.17
G_{12}	1.0 GPa for SWNT ropes diameter ~20 nm 6.0 GPa for SWNT ropes diameter < 4.5 nm
Density ρ	1.3 g/cm ³

The rule of mixtures gives the theoretical modulus of the composite fiber as

$$E_{\text{fiber}} = V_{\text{SWNT}} * E_{\text{SWNT}} + V_{\text{PAN}} * E_{\text{PAN}}, \quad (3.9)$$

where, V_{SWNT} and V_{PAN} are volume fractions of SWNTs and PAN in the composite fiber, E_{SWNT} and E_{PAN} are the moduli of SWNTs and PAN, and E_{Fiber} is the modulus of

composite fiber. The theoretical and experimental modulus values for the fiber are listed in Table 3.5.

From Table 3.5, we see that the experimental fiber modulus for non-acid treated SWNT/PAN fiber is 13.0 GPa, which is in the predicted range of 10.6 to 21.2 GPa; similarly for the acid treated SWNT/PAN fiber, the experimental modulus of 17.8 GPa is in the predicted range of 11.9 to 22.9 GPa. This suggests that the reinforcement effect of SWNTs in the composite fiber is in agreement with theoretical prediction.

Table 3.5 Comparison of experimental data and predicted values

	Non-Acid Treated SWNT/PAN				Acid Treated SWNT/PAN			
	rope diameter > 20 nm		rope diameter < 4.5 nm		rope diameter > 20 nm		rope diameter < 4.5 nm	
	PAN	SWNT	PAN	SWNT	PAN	SWNT	PAN	SWNT
f	0.540	0.982	0.540	0.982	0.600	0.984	0.600	0.984
$E_{\text{eff}}(\text{GPa})$	7.3	74.7	7.30	285.3	8.1	82.73	8.1	303.93
$E_{\text{fiber}}(\text{GPa})$	10.6		21.2		11.9		22.9	
$E_{\text{exp}}(\text{GPa})$	13.0				17.8			

3.4 Benzonitrile Functionalized SWNT/PAN Composite Fiber

The benzonitrile functionalized SWNT/PAN fibers have also been characterized using the same methods described in Section 3.1. The results are discussed below.

3.4.1 Geometric Properties

The SWNT weight percentage is 0.2% JS-2-88/PAN and JLH-II-085/PAN fibers. The photographs of the spun benzonitrile functionalized SWNT/PAN fiber spools are shown in Figure 3.14. From this figure we see that the JS-2-88 fiber is not homogeneous in appearance, evidenced by some white regions on the fiber surface. This may be due to the phase separation of PAN and SWNTs during spinning and/or coagulation process. The SEM images of these fibers are given in Figure 3.15.

We noticed that the fiber cross sections are not circular; there are apparent voids in the fiber. This is because we used dry jet spinning, and the diffusion of the solvent has resulted in this morphology.

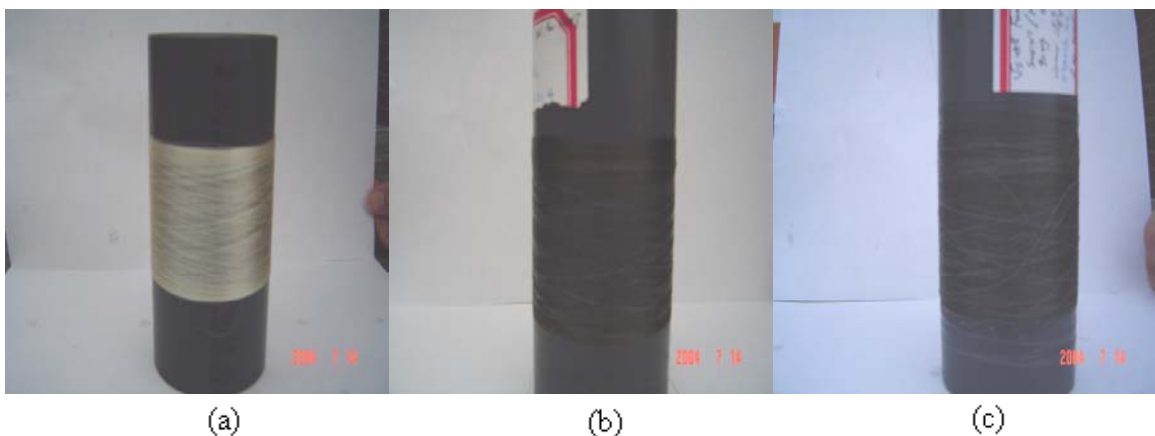


Figure 3.14 The Spools of (a) Exlan PAN, (b) JLH-II-085/PAN and (c) JS-2-88/PAN fiber.

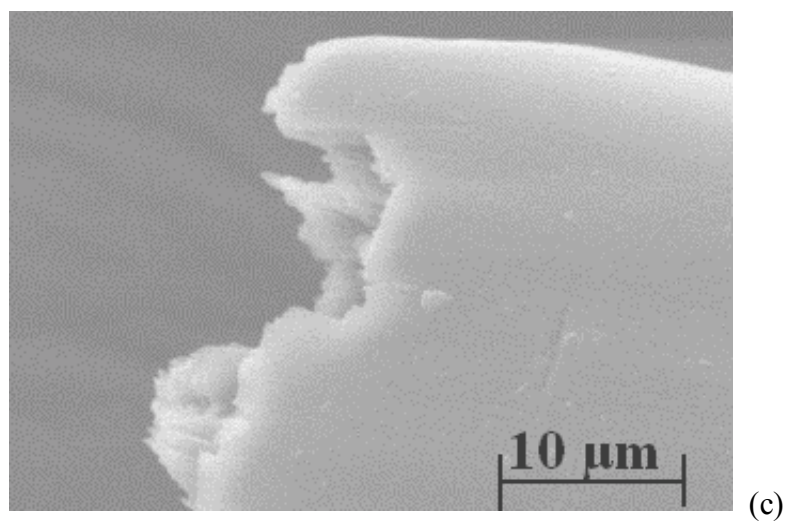
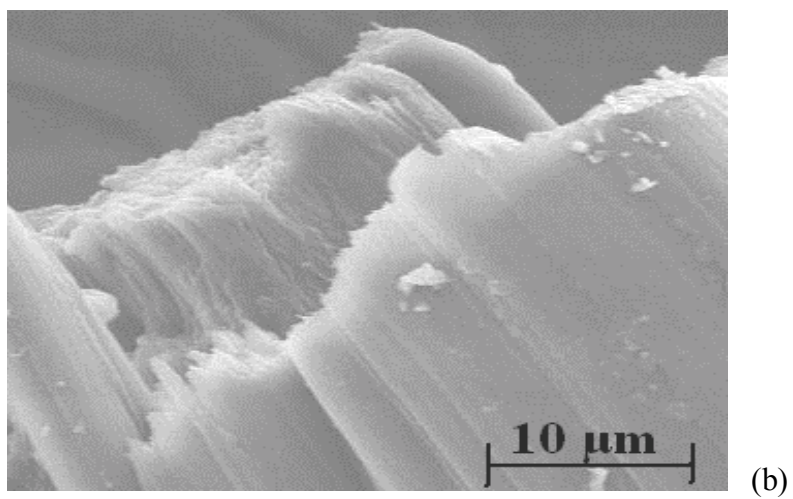
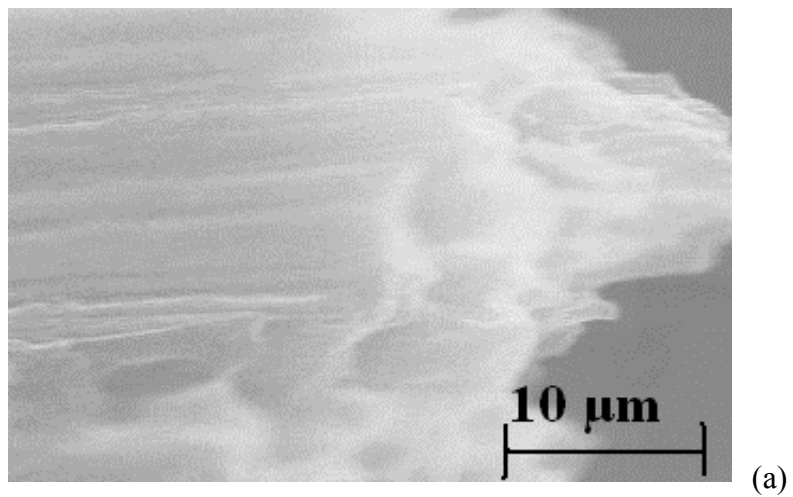


Figure 3.15 SEM image of functionalized fibers. (a) Exlan PAN, (b) JLH-II-085/PAN, (c) JS-2-88/PAN.

3.4.2 Tensile Test and Dynamic Mechanical Analysis

The tensile test results are given in Table 3.6. The dynamic mechanical properties of benzonitrile functionalized composite fibers are shown in Figures 3.16 and 3.17.

Table 3.6 Tensile properties of functionalized composite fibers

	Modulus (GPa)	Breaking Strength (GPa)	Breaking Elongation %
Exlan PAN_A	7.81 ± 0.03	0.25 ± 0.06	13 ± 3.0
JLH-II-085/PAN	7.82 ± 0.04	0.20 ± 0.03	8.3 ± 1.0
JS-2-88/PAN	7.30 ± 0.02	0.18 ± 0.04	10.2 ± 2.0

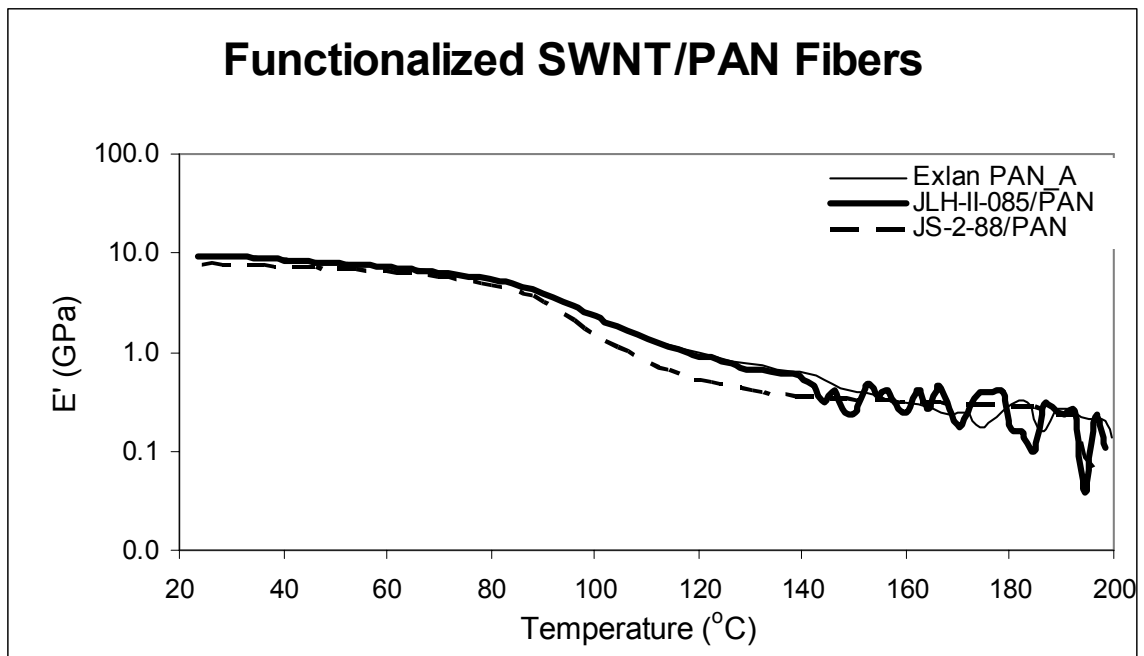


Figure 3.16 Storage modulus of benzonitrile functionalized SWNT/PAN fibers.

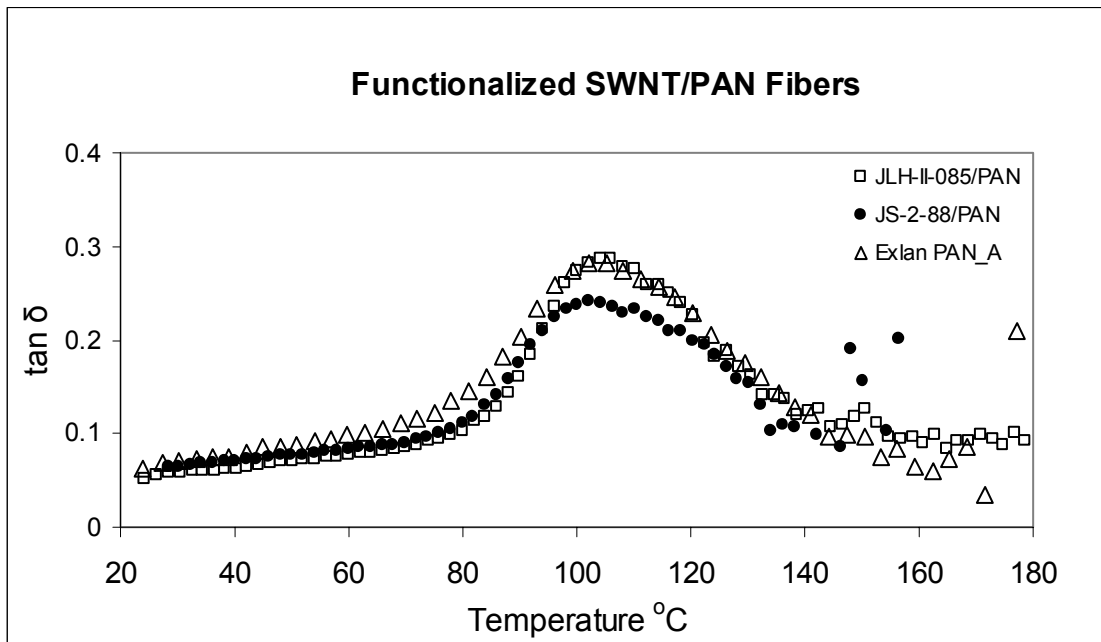


Figure 3.17 Loss tangent of functionalized SWNT/PAN fibers.

From the DMA and tensile tests, we see that there are no improvements in modulus and tensile strength. This can be attributed to the small percentage of SWNTs in the fiber, which is only 0.2wt%.

3.4.3 Thermo-Mechanical Analysis (Shrinkage)

The benzonitrile functionalized SWNT/PAN fiber shrinkage was determined using the TA Instruments thermo-mechanical analyzer (TMA 2940) at 0.2 MPa pre-stress. The heating rate was 10 °C/min. After heating from room temperature to 250 °C, the sample was kept at 250 °C for half an hour. The results are given in Figure 3.18.

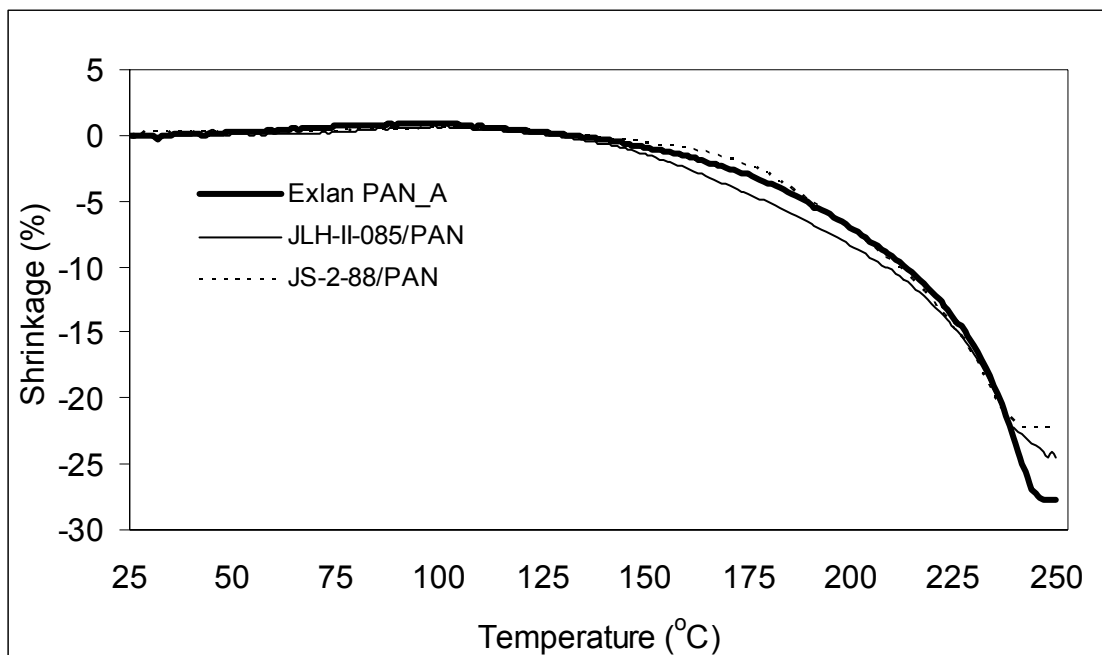


Figure 3.18 TMA of benzonitrile functionalized SWNT/PAN fibers.

From TMA results we see that these fibers shrinking just a little bit at 250°C. Even after heating for half an hour, they do not exhibit further shrinkage. This indicates they have already reached their thermal shrinkage limit. There are small differences in shrinkage behavior: JS-2-88 SWNT/PAN fiber has the least shrinkage, and the pure Exlan_PAN_A fiber has the largest thermal shrinkage. However, we cannot conclude that SWNTs have a significant effect on reducing thermal shrinkage for functionalized SWNT/PAN fibers. Compared to the thermal shrinkage of non acid treated SWNT/PAN fibers⁵⁸, these results are understandable, as SWNT content in thee samples is only 0.2%.

3.4.4 Thermo-gravimetric Analysis

The pure PAN, JLH-II-085/PAN, JS-2-88/PAN fiber were subjected to TGA study at 250 °C for 10 hours in air. Samples were heated from 25 °C to 250 °C at a rate of 10 °C/min and held at 250 °C. The results are shown in Figure 3.19.

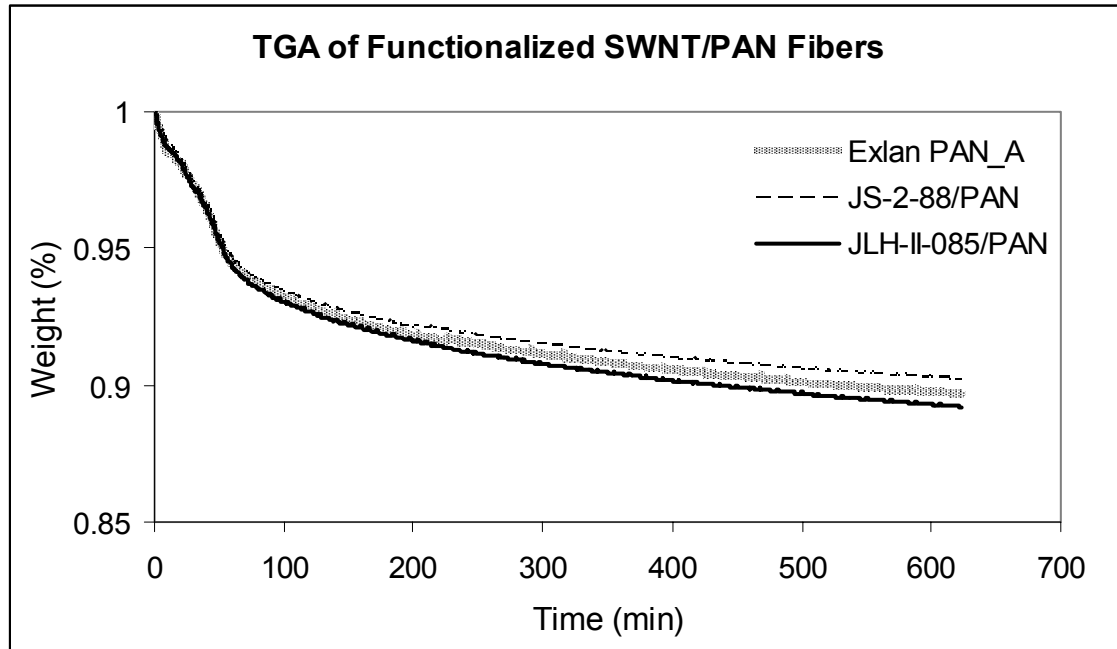


Figure 3.19 TGA test of functionalized SWNT/PAN fibers.

We did not observe any significant weight loss among these fibers. This indicates that adding 0.2% of functionalized SWNTs in PAN fiber does not have a significant oxidation retarding effect on the composite fibers.

3.4.5 Raman Spectra

The Raman Spectra of these functionalized SWNT/PAN fibers are given in Figure 3.20. We can see that Raman spectra of functionalized SWNTs are similar to the characteristic Raman spectra of SWNTs. This shows that the SWNT structure remains unchanged after functionalization treatment.

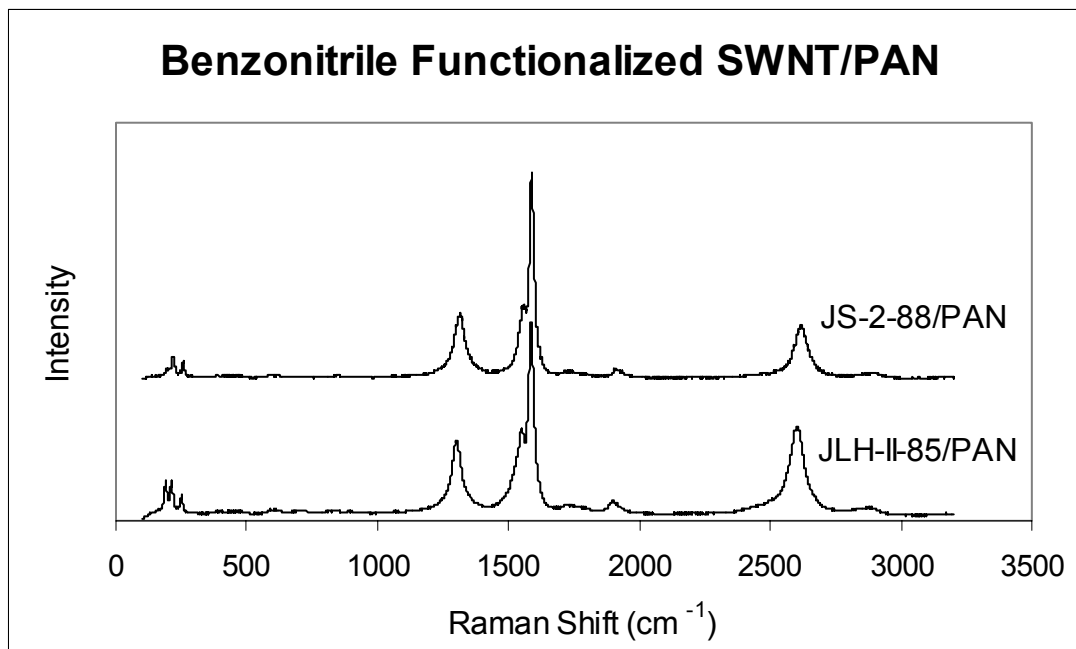


Figure 3.20 Raman spectra of functionalized SWNT/PN fibers.

3.4.6 WAXD

The wide angle x-ray diffraction patterns of pure Exlan PAN and benzonitrile functionalized SWNT/PAN fibers are shown in Figure 3.21

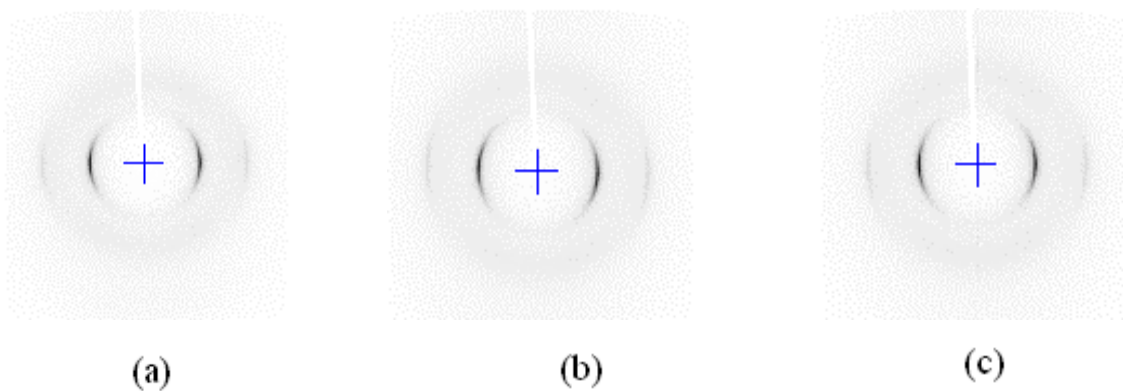


Figure 3.21 WAXD patterns of functionalized fibers. (a) Exlan PAN, (b) JLH-II-085/PAN, (c) JS-2-88/PAN.

The equatorial and azimuthal WAXD scans for these fibers are given in Figures 3.22 and 3.23. From equatorial WAXD scans we can calculate the PAN lattice parameters. The PAN crystal lattice parameter results are given in Table 3.7.

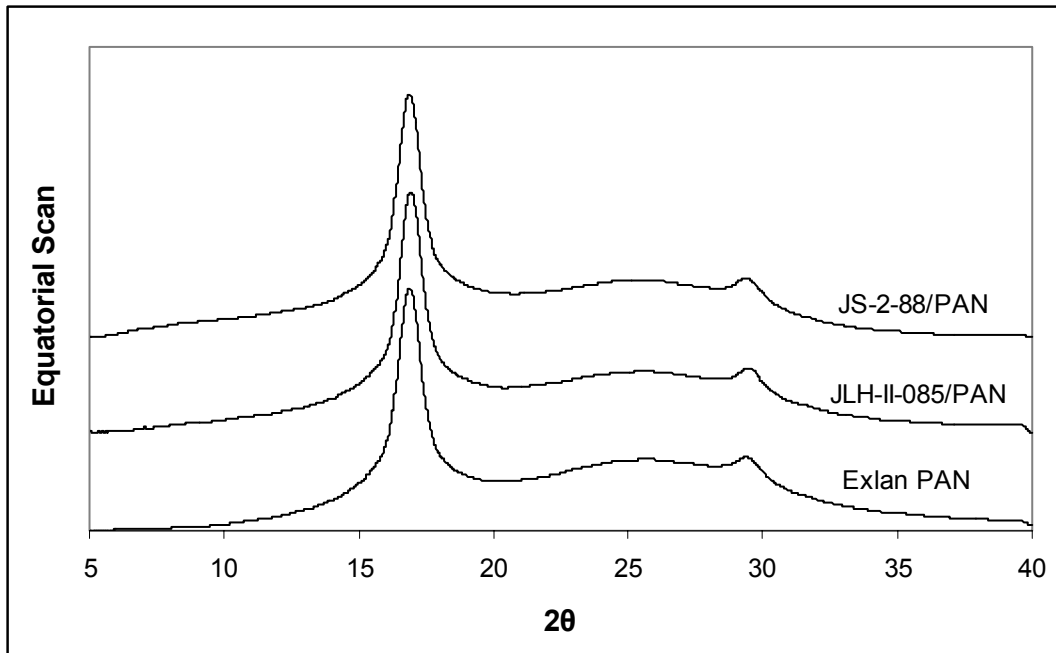


Figure 3.22 Equatorial WAXD scan of functionalized SWNT/PAN fibers.

From the equatorial scan, we can determine the lattice parameters of these three fibers. The results are listed in Table 3.7. The PAN lattice parameters are similar for these three types of fibers, meaning that the 0.2% functionalized SWNTs do not have much influence on the crystal morphology of PAN.

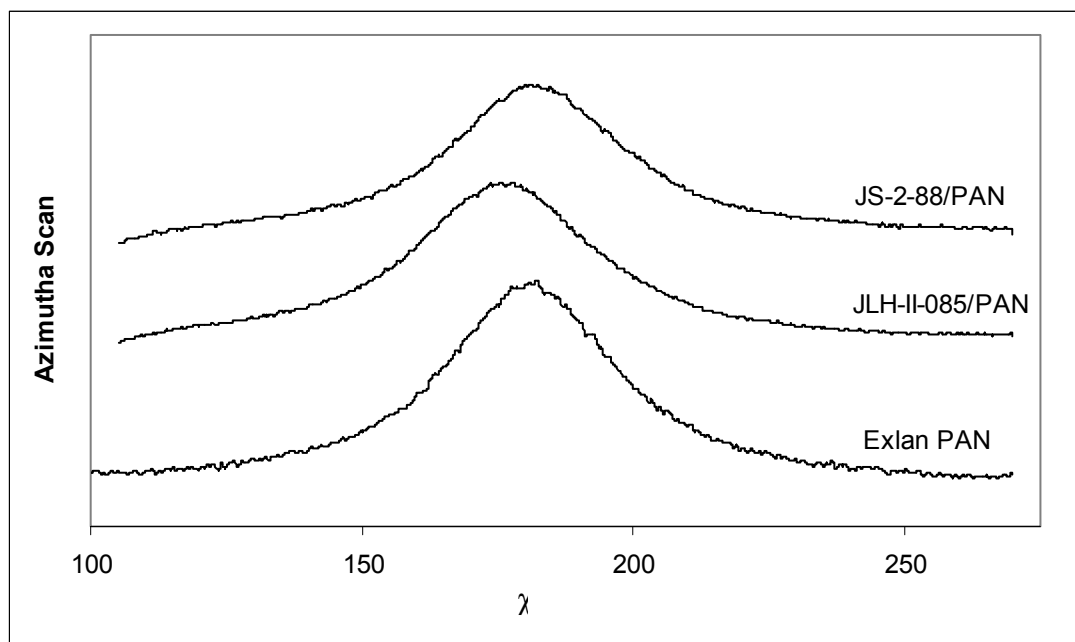


Figure 3.23 Azimuthal WAXD scan of functionalized SWNT/PAN fibers.

Table 3.7 Lattice parameters of Functionalized SWNT/PAN Fibers

	Plane (10)			
	2θ	d-spacing (Å)	FWHM	Crystal Size (Å)
Exlan PAN	16.91°	5.24	0.83°	97
Js-2-88 /PAN	16.88°	5.25	0.83°	100
JLH-II-085/PAN	16.91°	5.24	0.79°	96

CHAPTER 4 CONCLUSIONS AND RECOMMENDATIONS

4.1 Conclusions

Sonication is currently the most efficient method to disperse SWNT bundles in DMF. The SWNTs in SWNT/PAN composite fibers have high orientation, with a Herman's orientation factor of about 0.98. This indicates that with draw ratio of about 6 in the spinning process, SWNTs can be well aligned in the composite fiber.

The SWNT weight percentage in the composite fiber is an important factor to consider. In our case, 0.2 wt% functionalized SWNTs does not show a significant improvement effect, while composite fibers with 5 wt % SWNTs have shown great property improvements. For composite fibers with 5 wt% SWNTs, the tensile modulus of SWNT/PAN fiber have increased dramatically as compared to the pure PAN fiber, from 5.9 GPa to 13.0 GPa. The tensile strength increased from 0.23 GPa to 0.33 GPa. The DMA experiments also showed the increased storage modulus property for SWNT/PAN composite fibers. The magnitude of loss tangent peak decreased correspondingly. The broadening of the loss tangent peak for non-acid treated SWNT/PAN fibers is evidence of SWNT/PAN interaction.

The thermal shrinkage at 200 °C for SWNT/PAN composite fiber is about 14%, less than half of the shrinkage of the control PAN fiber. This result is consistent with the DMA results and suggests that the presence of SWNTs have a hindrance effect on the segmental motion of PAN molecule chains.

After moderate nitric acid treatment, most of the SWNTs still keep their original structure, which can be confirmed by FTIR and Raman Spectra results. At the same time some extra functional groups, such as $-C=O$ or $-COOH$, may have been added to the SWNTs. The small shift of G band peak position may be evidence of the addition of these groups. On the other hand, the mechanical properties of the acid treated SWNT/PAN composite fiber are further improved: modulus increased from 13.0 GPa to 17.8 GPa and tensile strength increased from 0.33 GPa to 0.45 GPa, a nearly 30% improvement compared to non-acid treated SWNT/PAN composite fibers. This shows that nitric acid treatment further improved the fiber properties.

As for benzonitrile functionalized SWNT/PAN, we did not see tensile or DMA property improvements, however, we do see some degree of reduction in thermal shrinkage, considering the low content (0.2%) of SWNTs in the composite fiber.

4.2 Recommendations for Future Work

First, we need to find a quantitative method to characterize the degree of dispersion and exfoliation of SWNTs. Only with a quantitative dispersion characterization method can we compare and seek more efficient processing methods to disperse and exfoliate SWNTs. We need to know, to what extent sonication, stirring, compounding can disperse SWNTs.

Secondly, we need to understand the morphology of SWNT/PAN mixture systems. SWNTs' influence on molecular mobility of PAN is necessary to further investigate the mechanical behavior of SWNT/PAN composite fibers.

Thirdly, the reinforcement mechanism, such as load distribution and deformation process, is also very important in structural design of high performance composite fibers.

Since the fiber quality depends largely on the rheological properties of SWNT/PAN dope, the influence of SWNTs on dope rheology is an important issue. SWNTs have already shown their reinforcement effects in composite fibers. However, to fully exploit their extraordinary properties, we have to develop optimal processing methods and understand their reinforcement mechanisms in greater depth.

APPENDIX A: MATLAB PROGRAM FOR CALCULATING SWNTS ORIENTATION FUNCTION FROM RAMAN SPECTRA

```

function raman_vv
clc
clear
w = [5:5:180];
%phi=[0,14,27,45,63,76,90];
%vv=[1075 1008 868 596 432 335 330]
%[1075 1008 868 596 432 335 330]
%[1081 996 863 581 349 283 268]

%phi=[0,5,10,15,25,35,45,55,65,75,85,90];
%vv=[3779 3809 3679 3006 2087 1330 717 380 148 84 73
79] % Non acid Treated
%vv=[3965 3825 3773 3419 3152 2721 2661 2019 1210 668 325
125] % Acid Treated

phi=[ 0 5 10 20 30 45 60 85 90]
vv=[3291+80 2980+80 2898+80 2333+80 1602+80 529+80 118+80 84 80 ] %
Non Acid Treated

phi=[ 0 15 25 35 45 55 65 75 90]
vv=[3581+80 2578+80 1911+80 1100+80 609+80 296+80 121+80 48+80 9+80]

vv1=vv/vv(1);
vv1

leastsquare=zeros(size(w,2),2);

vvc = zeros(size(w,2),size(phi,2));

for index_w = 1:size(w,2)
    for index_phi = 1:size(phi,2)

        vvc(index_w,index_phi)
=dblquad(@vvraman,0,180,0,360,0.001,[],phi(index_phi),w(index_w));
        end
    end

for index_w = 1:size(w,2)
    vvcl(index_w,:) =vvc(index_w,:)/vvc(index_w,1);
end
vvcl

for i = 1:size(w,2)
    leastsquare(i,1)=w(i);
    leastsquare(i,2)=sum((vvcl(i,:)-vv1).^2);
end

```

```

leastsquare
[x y]=min(leastsquare(:,2));
min_w=leastsquare(y,1);
min_w

avgcossqrth=quad(@cos2sum,0,180,[],[],min_w)/quad(@gaussian,0,180,[],[]
,min_w)
f=(3*avgcossqrth-1)/2
%
function Y=cos2sum(th,w)
Y=sin(th./180*pi).*((cos(th./180*pi)).^2).*exp(-
4*log(2)*(th./180*pi./(w/180*pi)).^2);

function Y=gaussian(th,w)
Y= sin(th./180*pi).*exp(-4*log(2)*(th./180*pi./(w/180*pi)).^2);

function Y=vvraman(th,zhi,phi,w)
Y= sin(th./180*pi).*((cos(phi./180*pi).*cos(th./180*pi)-
sin(th./180*pi).*sin(phi./180*pi).*sin(zhi./180*pi)).^4).*exp(-
4*log(2)*(th./180*pi./(w/180*pi)).^2);
%

End

```

REFERENCES

- ¹ A. K. Lau, D. Hui, *Composites: Part B: Engineering*, 33, 4,, 2002, p263-277.
- ² T. W. Ebbesen, *Carbon nanotubes: preparation and properties*, CRC Press, 1997, p12.
- ³ T. W. Ebbesen, *Carbon nanotubes: preparation and properties*, CRC Press, 1997, p12.
- ⁴ Wyckoff, *Crystal Structure*, VI. 1, Interscience Inc, New York, 1964.
- ⁵ R.Bacon, *J. Appl. Phys.*, 31, 283, 1960, p26.
- ⁶ R. D. Heidenreich, *J. Appl. Crstallogr.* 1, 1, 1968, p43.
- ⁷ J. S. Speck, *Structural Correlations in Graphite and Its Layer Compounds*, Ph.D. Thesis, MIT, 1989.
- ⁸ H.W. Kroto, J.R. Heath, S.C. O'Brien, R.F. Curl, R. E. Smalley, *Nature*, 318, 6042, 1985, p162.
- ⁹ S. Iijima, *Nature*, 354, 6348, 1991, p56.
- ¹⁰ M S, Dresselhaus, G. Dresselhaus , P. Avouris, *Carbon nanotubes: synthesis, structure, properties and applications*, Springer, 2001.
- ¹¹ T. W. Odom, J.L. Huang, P. Kim, C. M. Lieber, *Nature*, 391, 6662, 1998, p62.
- ¹² N. Hamada, S.Sawada, A. Oshiyama, *Phys. Rev. Lett.* 68, 10, 1992, p1579.
- ¹³ S.Bandow, S.Asaka, Y. Saito, A. M. Rao, L.Grigrorian, E. Richter, P. C. Eklund, *Physical Rev. Lett.*, 80, 17, 1998, p3779.
- ¹⁴ A. Thess, R. Lee, P. Nikolaev, H. Dai, P. Petit, J. Robert, C. Xu, Y. H. Lee, S. G. Kim, A.G. Rinzler, D. T. Colbert, G. E. Scuseria, D. Tombnek, J. E. Fischer, R. E. Smalley, *Science*, 273, 5274, 1996, p83
- ¹⁵ J. P. Lu, *Phys. Rev. Lett.*, 79,7, 1997, p1297.
- ¹⁶ R. S. Ruoff, D. C. Lorents, *Carbon*, 33, 7, 1995, p925.

- ¹⁷ J. P. Salvetat, G. A. D. Briggs, J. M. Bonard, R. R. Bacsa, A. J. Kulik, T. Stöckli, N. A. Burnham, L. Forró, *Phys. Rev. Lett.*, 82, 5, 1999, p944.
- ¹⁸ T. Spires, R. M. Brown, High Resolution TEM Observations of Single-Walled Carbon Nanotubes, Location:
<http://www.botany.utexas.edu/facstaff/facpages/mbrown/ongres/tspires/nano.htm>.
- ¹⁹ A. Thess, R. Lee, P. Nikolaev, H. Dai, P. Petit, J. Robert, C. Xu, Y. H. Lee, S. G. Kim, A.G. Rinzler, D. T. Colbert, G. E. Scuseria, D. Tombnek, J. E. Fischer, R. E. Smalley, *Science*, 273, 5274, 1996, p83.
- ²⁰ C. Dekker, *Physics Today*, 52, 5, 1999, p22.
- ²¹ J. Hone, M. Whitney, A. Zettle, *Synthetic Metals*, 103, 3, 1999, p2498.
- ²² M. F. Yu, F. S. Bradley, S. Arepalli, R. S. Ruoff, *Phys. Rev. Lett.* 84, 24, 2000, p5552.
- ²³ P. M. Ajayan, L. S. Schadler, C. Giannaris, A. Rubio, *J. Appl. Polym. Sci.*, 92, 5, 2004, p3394.
- ²⁴ S. Yang, J. R. Castilleja, E. V. Barrera, K. Lozano, *Polymer Degradation and Stability*, 83, 3, 2004, p383.
- ²⁵ T. V. Sreekumar, T. Liu, B. G. Min, H. Guo, S. Kumar, R. H. Hauge, R. E. Smalley, *Adv. Mater.*, 16, 1, 2004, p58-61.
- ²⁶ J. S. Bunch, T. N. Rhodin, P. L. McEuen, *Nanotechnology*, 15, 2, 2004, pS76.
- ²⁷ N. Choi, U. Takayuki, N. Hidehiro, I. Takao, M. Wataru, A. Seiji, N. Yoshikazu, I. Mitsuru, T. Hiroshi, *Jap. J. Appl. Phys., Part 1*, 39, 6 B, 2000, p3707.
- ²⁸ C. Y. Liu, A. J. Bard, F. Wudl, I. Weitz, J. R. Heath, *Electrochemical and Solid-State Letters*, 2, 11, 1999, p577.
- ²⁹ T. Liu, T.V. Sreekumar, S. Kumar, R.H. Hauge, R. E. Smalley, *Carbon*, 41, 12, 2003, p2440.
- ³⁰ T.W. G. aham Solomons, *Organic Chemistry*, John Wiley & Sons, 6th Edition, p405, 1996.
- ³¹ B. Barr, R.N. Swamy, *Fiber Reinforced Concrete*, Elsevier Applied Science, 1989, p27.
- ³² J. B. Donnet, T. K. Wang, J. C. M. Peng, S. Ribouillat, *Carbon Fibers*, Marcel Dekker; 3rd edition, 1998.

- ³³ Vincent Kelly, Carbon fiber: manufacture and applications, Elsevier, 2004.
- ³⁴ L.S. Schadler, S.C. Giannaris, P.M Ajayan, Appl. Phys. Lett. 73, 26, 1998, p3842.
- ³⁵ X. Zhang, T. Liu, T. V. Sreekumar, S. Kumar, V. C. Moore, R. H. Hauge, R. E. Smalley, Nano Lett. 3, 9, 2003, p1285-1288.
- ³⁶ B. Sarbajit, S. S. Wong, J. Phys. Chem. B, 106, 47, 2002, p12144.
- ³⁷ I. W. Chiang, B. E. Brinson, R. E. Smalley, J. L. Margrave, and R. H. Hauge, J. Phys. Chem. B., 105, 6, 2001, p1157.
- ³⁸ A. G. Rinzler, J. Liu, H. Dai, P. Nikolaev, C. B Huffman, F. J. Rodriguez-Macias, P. J. Boul, A. H. Lu, D. Heymann, D. T. Colbert, R. S. Lee, J. E. Fischer, A. M. Rao, P. C. Eklund, R. E. Smalley, Appl. Phys. A, 67, 1, 1998, p29.
- ³⁹ C. Bower, A. Kleinhammes, Y. Wu, O. Zhou, Chem. Phys. Lett., 288, 2-4, 1998, p481.
- ⁴⁰ H. Hu, B. Zhao, M. Itkis, R. C. Haddon, J. Phys. Chem. B, 107, 50, 2003, p13838.
- ⁴¹ P. Nikolaev, M. J. Bronikowski, R. K. Bradley, F. Rohmund, D. T. Colbert, K. A. Smith, R. E. Smalley, Chem. Phys. Lett, 313, 1-2, 1999, p91.
- ⁴² I. W. Chiang, B. E. Brinson, A. Y. Huang, P. A. Willis, M. J. Bronikowski, J. L. Margrave, R. E. Smalley, R. H. Hauge, J. Phys Chem. B, 105, 35, 2001, p8297.
- ⁴³ I. W. Chiang, B. E. Brinson, R. E. Smalley, J. L. Margrave, and R. H. Hauge, J. Phys. Chem. B., 105, 6, 2001, p1157.
- ⁴⁴ M. J. O'Connell, S. M. Bachilo, C. B. Huffman, V. C. Moore, M. S. Strano, E. H. Haroz, K. L. Rialon, P. J. Bout, W. H. Noon, C. Kittrell, J. Ma, R. H. Hauge, R. B. Weisma, R. E. Smalley, Science, 297, 5581, 2002, p593.
- ⁴⁵ C. A. Dyke, J. M. Tour, Chemistry - A European Journal, 10, 4, 2004, p812.
- ⁴⁶ D. Renjith, C. P. R. Nair, K. N. Ninan, Polymer International, 52, 9, 2003, p1519
- ⁴⁷ T. V. Sreekumar, T. Liu, B. G. Min, H. Guo, S. Kumar, R. H. Hauge, R. E. Smalley, Adv. Mater., 16, 1, 2004, p58..
- ⁴⁸ M. Cardona, R. M. Martin, L. M. Falicov, Topics of Applied Physics, Springer-Verlag, 8, 1983, p79.

- ⁴⁹ A. Jorio, M. A. Pimenta, A. G. S. Filho, R Saito, G. Dresselhaus, M. S. Dresselhaus, *New J. Phys.* 5, 139, 2003, p1.
- ⁵⁰ I. W. Chiang, B. E. Brinson, R. E. Smalley, J. L. Margrave, R. H. Hauge, *J. Phys. Chem. B.*, 105, 6, 2001, p11571.
- ⁵¹ P. Whelan, J. Abraham, A. Hirsch, R. Graubner, A. Dizakova, F. Hennrich, M. Kappes, J. Forsyth, *AIP Conference Proceedings*, 685, 1, 2003, p189.
- ⁵² X. D Liu, W. Ruland, *Macromolecules*, 26, 12, 1993, p3030.
- ⁵³ P. Rizzo, A. Finizia, G. Gaetano, P. Vittorio, C. Paolo, *Macromolecules*, 29, 27, 1996, p8852.
- ⁵⁴ J. Brandrup, E. H. Immergut, E. A. Grulke, A. Abe, D. R. Bloch, *Polymer Handbook*, Interscience Publishers, 1966.
- ⁵⁵ R. Haggemueller, H. H. Gommans, A. G. Rinzler, J. E. Fischer, K. I. Winey, *Chem. Phys. Lett.* 330, 3-4, 2000, p219.
- ⁵⁶ T. Liu, S. Kumar, *Chem Phys Lett.* 378, 3-4, 2003, p257.
- ⁵⁷ I. M. Ward, D. W. Hadley, *An Introduction to the Mechanical Properties of Solid Polymers*; John Wiley & Sons, 1995, p300.
- ⁵⁸ T. V. Sreekumar, T. Liu, B. G. Min, H. Guo, S. Kumar, R. H. Hauge, R. E. Smalley, *Adv. Mater.*, 16, 1, 2004, p58.